



<b>Customer</b>	: ESRIN	<b>Document Ref</b>	: SST_CCI-REP-UKMO-001
<b>WP No</b>	:	<b>Issue Date</b>	: 15 February 2013
		<b>Issue</b>	: C

**Project** : CCI Phase 1 (SST)

**Title** : Improvements to the Operational Sea Surface Temperature and Sea Ice Analysis (OSTIA) system

**Abstract** : The Operational Sea Surface Temperature (SST) and Sea Ice Analysis (OSTIA) system was developed at the Met Office where it is run in near-real time (NRT) daily. An OSTIA reanalysis system has previously been developed based largely on the NRT system. An updated version of this reanalysis system will be used in phase 1 of the CCI SST project to produce a new global gridded SST analysis on a 0.05° grid with no data gaps (known as a 'Level 4' data product). This report describes the work that has been carried out at the Met Office, to develop the OSTIA reanalysis system with the aim of improving the CCI reanalysis Level 4 product. New background error covariances have been calculated which improve the accuracy of the SST analysis. Also, the use of sea ice data in the system has been enhanced.

**Author** :   
 \_\_\_\_\_  
 Jonah Roberts-Jones, Emma Fiedler, Matthew Martin, Alison McLaren, Met Office

**Approved** :   
 \_\_\_\_\_  
 Chris Merchant  
 Science Leader  
 University of Edinburgh

**Accepted** : \_\_\_\_\_  
 Craig Donlon  
 ESA Technical Officer

**Distribution** : SST\_cci team members  
 ESA (Craig Donlon)

**EUROPEAN SPACE AGENCY  
 CONTRACT REPORT**

The work described in this report was done under ESA contract. Responsibility for the contents resides in the author or organisation that prepared it.



## AMENDMENT RECORD

This document shall be amended by releasing a new edition of the document in its entirety. The Amendment Record Sheet below records the history and issue status of this document.

### AMENDMENT RECORD SHEET

ISSUE	DATE	REASON FOR CHANGE
A	2013-01-15	Initial Issue
B	2013-01-16	Updated after internal review
C	2013-02-15	Corrections to Section 4

## TABLE OF CONTENTS

<b>1. INTRODUCTION.....</b>	<b>4</b>
1.1 Purpose and Scope.....	4
1.2 Referenced Documents .....	4
1.3 Definitions of Terms .....	5
<b>2. NEW BACKGROUND ERROR COVARIANCES .....</b>	<b>7</b>
2.1 Introduction.....	7
2.1.1 Purpose of algorithm.....	7
2.2 Algorithm Description for deriving new background covariances .....	8
2.2.1 Algorithm Overview.....	8
2.2.2 Theoretical Description .....	8
2.2.3 Processing Outline.....	8
2.3 Results .....	10
2.3.1 AATSR observation-minus-background results.....	10
2.3.2 Drifter observation-minus-background results.....	12
2.3.3 AATSR Seasonal observation-minus-background results .....	15
2.3.4 AATSR anisotropic observation-minus-background results .....	17
2.4 Implementation.....	20
2.5 Assumptions and limitations.....	24
2.5.1 Algorithm performance .....	24
2.6 Conclusions.....	25
2.7 Future Enhancements.....	26
2.7.1 Enhancement 1.....	26
<b>3. SEA ICE AND SST CONSISTENCY.....</b>	<b>27</b>
3.1 Introduction.....	27
3.2 Methods.....	27
3.3 Results .....	28
3.3.1 Timeseries .....	28
3.3.2 SST and Sea Ice Scatter Plots .....	29
3.4 Conclusions.....	31
3.5 Future Enhancements.....	32
<b>4. PRE-PROCESSING SEA ICE DATA .....</b>	<b>33</b>
4.1 Introduction.....	33
4.2 Method .....	33
4.3 Results .....	34
4.4 Conclusions.....	35
4.5 Assumptions and Limitations .....	35
4.6 Future Enhancements.....	35
<b>5. USE OF SEA ICE DATA AUXILIARY INFORMATION .....</b>	<b>36</b>
5.1 Error Estimates.....	36
5.1.1 Background.....	36
5.1.2 Method.....	36
5.1.3 Assumptions and Limitations .....	36
5.1.4 Conclusions .....	37
5.2 Status Flags .....	37
5.2.1 Background.....	37
5.2.2 2m air temperature flag.....	38
5.2.3 Coastal correction method.....	39
5.2.4 Lake ice flag.....	39
5.2.5 Conclusions .....	39
<b>6. SUMMARY.....</b>	<b>40</b>

## 1. INTRODUCTION

### 1.1 Purpose and Scope

The Operational Sea Surface Temperature (SST) and Sea Ice Analysis (OSTIA) system was developed at the Met Office where it is run in near-real time (NRT) daily [RD.213]. OSTIA uses satellite and in-situ SST data, together with sea ice concentration data, to produce a global gridded SST analysis on a 0.05° grid with no data gaps (known as a 'Level 4' data product). An OSTIA reanalysis system has been developed largely based on the NRT system and has been used to produce a SST reanalysis for the period 1985 to 2007 (OSTIA reanalysis v1.0) [RD.239]. This reanalysis system will be used in the phase 1 of the CCI SST project to produce the Level 4 product using satellite data only [RD.175]. The analysis process in OSTIA is not described in detail here; instead the reader is referred to recent OSTIA publications [RD.213, RD.239].

This report details recent work done by the Met Office to improve the OSTIA reanalysis system for the CCI SST project. OSTIA uses a background error covariance field to determine how observation increments are spread into the background field. Previously, these error estimates were calculated from model results as described in [RD.213]. Development work has been carried out to improve these fields by calculating the background error field using observation-minus-background differences from the Along Track Scanning Radiometer (ATSR) and drifter data obtained from the OSTIA reanalysis v1.0. This development work is described here together with results from a series of experiments to assess the impact on the accuracy of the SST analysis. Further tests were made to investigate the impact of increasing the number of analysis iterations and also withholding in-situ data from the analysis (as satellite data will only be used for the CCI level 4 product).

In addition to developing the SST analysis, there is also the potential to improve the use of sea ice data in OSTIA. Analysis of the OSTIA reanalysis v1.0 showed some inconsistency between the sea ice data and SST data around the ice edge [RD.239] and this is further investigated here. A new pre-processing method to fill in missing data gaps in the sea ice data has been developed and is assessed. Finally, the report documents how the auxiliary data provided with the sea ice data will be used in the OSTIA reanalysis CCI product.

### 1.2 Referenced Documents

The following is a list of documents with a direct bearing on the content of this report. Where referenced in the text, these are identified as RD.n, where 'n' is the number in the list below:

- RD.43 Eastwood S., K. R. Larsen, T. Lavergne, E. Nielsen, and R. Tonboe (2010), Global Sea Ice Concentration Reprocessing Product User Manual, Met Norway/Danish Meteorological Institute, EUMETSAT Ocean and Sea Ice SAF.
- RD.74 Rayner, N. A., D. E. Parker, E. B. Horton, C. K. Folland, L. V. Alexander, D. P. Rowell, E. C. Kent, and A. Kaplan (2003), Global analyses of sea surface temperature, sea ice, and night marine air temperature since the late nineteenth century. *J. Geophys. Res.*, 108(D14):4407, DOI: 10.1029/2002JD002670.
- RD.175 CCI Phase 1 (SST), Product Specification Document, SST\_CCI-PSD-UKMO-001 Issue\_2

- RD.213 Donlon, C.J., M. Martin, J. Stark, J. Roberts-Jones, E. Fiedler and W. Wimmer (2012). The Operational Sea Surface Temperature and Sea Ice Analysis (OSTIA) system, *Remote Sensing of the Environment*, 116, 140-158.
- RD.239 Roberts-Jones, J., Fiedler, E. K. and M. Martin (2012), Daily, global, high-resolution SST and sea-ice reanalysis for 1985-2007 using the OSTIA system, *J. Climate*, doi:10.1175/JCLI-D-11-00648.1, in press.
- RD.275 Roberts-Jones, J., Fiedler, E. K. and M. Martin (2011), Met Office Technical Report 561: Description and assessment of the OSTIA reanalysis, Met Office.
- RD.276 Daley, R. (1991), *Atmospheric data analysis*. Cambridge University Press.
- RD.277 Steele, M., R. Morley, and W. Ermold (2001), PHC: A global ocean hydrography with a high-quality Arctic Ocean, *J. Climate*, 14, 2079–2087.
- RD.278 Hollingsworth, A. and P. Lonnberg (1986). The statistical structure of short-range forecast errors as determined from radiosonde data, *Tellus*, 38A, 111-136.
- RD.279 Bell, M.J., R.M. Forbes and A. Hines (2000), Assessment of the FOAM global data assimilation system for real-time operational ocean forecasting, *Journal of Marine Systems*, 25, 1-22.
- RD.280 Bell, M.J., A. Hines and M.J. Martin (2003), Variational assimilation evolving individual observations and their error estimates. Met Office Ocean Applications technical note no.32, available from Met Office, FitzRoy Road, Exeter. UK.
- RD.281 Hurrell, J. W., J. J. Hack, D. Shea, J. M. Caron, and J. Rosinski (2008). A new sea surface temperature and sea ice boundary dataset for the Community Atmosphere Model, *J. Climate*, 21, 5145-5153.
- RD.282 Ingleby, B., and M. Huddleston (2007), Quality control of ocean temperature and salinity profiles - historical and real-time data. *Journal of Marine Systems*, 65, 158-175.
- RD.283 K.S. Mogensen, M.A. Balmaseda, A. Weaver, M.J. Martin, A. Vidard, (2009). NEMOVAR: A variational data assimilation system for the NEMO ocean model. ECMWF newsletter, Summer 2009.
- RD.284 Mogensen, K., M. Alonso Balmaseda, A. Weaver, 2012. The NEMOVAR ocean data assimilation system as implemented in the ECMWF ocean analysis for System 4. ECMWF tech memo number 668. February 2012.
- RD.285 CCI Phase 1 (SST), Users Requirements Document, SST\_CCI-URD-UKMO-001 Issue\_2,

### 1.3 Definitions of Terms

The following terms have been used in this report with the meanings shown.

Term	Definition
(A)ATSR	(Advanced) Along Track Scanning Radiometer

ARGO	Global array of observational profiling floats
CCI	Climate Change Initiative
DJF	December, January, February
EN3	Quality controlled subsurface temperature and salinity data set [RD.282]
GCOS	Global Climate Observing System
HadISST1	Met Office Hadley Centre Sea Ice and Sea Surface Temperature data set (version 1)
JJA	June, July, August
NRT	Near Real Time
O-B	Observation minus Background
OSI-SAF	Ocean and Sea Ice Satellite Application Facility (EUMETSAT)
OSTIA	Operational Sea Surface Temperature and Sea Ice Analysis
QC	Quality Control
RMSE	Root Mean Square Error
SST	Sea Surface Temperature

## 2. NEW BACKGROUND ERROR COVARIANCES

### 2.1 Introduction

The OSTIA system assimilates SST observations onto a background field based on persistence of the previous day's SST analysis with some relaxation to climatology. The weight and degree to which an observation is spread in this assimilation is dependent on both the observation error covariance matrix and the background error covariance matrix in the Optimal Interpolation (O.I.) equation [RD.213]. Within the OSTIA SST assimilation, the observation errors are assumed to be spatially uncorrelated so the spatial spreading of an observation is wholly determined by the background error covariance matrix, see [RD.213] for a full description of the OSTIA SST assimilation scheme.

The background error covariance matrix is too large to specify explicitly. It is parameterised into a diagonal matrix of background error variances with the off-diagonal elements specified using a second-order auto-regressive (SOAR) function which spatially correlates the background errors. The background error variance and background error correlation length scales parameters are estimated using the Hollingsworth and Lonnerberg technique [RD.278].

A more realistic representation of the background errors is achieved through decomposing the background errors into small scale errors associated with mesoscale ocean variability, hereafter referred to as mesoscale background errors, and larger scale background errors that occur over the scale of atmospheric synoptic systems, hereafter referred to as synoptic scale background errors [RD.280]. Each component of the background error will have an associated error variance and error correlation length scale, these will combine to give the total background error variance and an effective correlation length scale. The estimation procedure employed here is designed to decompose the background error into errors associated with the two scales and estimate both the mesoscale and synoptic scale error variance parameters.

The Hollingsworth and Lonnerberg method uses observation-minus-background (o-b) differences to estimate the background error covariance parameters. Observation-minus-background differences from the OSTIA reanalysis v1.0 [RD.239] for the in situ and (Advanced) Along Track Scanning Radiometer ((A)ATSR) observations were used in the estimates presented here.

Section 2.2 describes the Hollingsworth and Lonnerberg technique and provides a description of the processing outline. Section 2.3 presents results of the background error estimates from the AATSR o-b differences (sections 2.3.1, 2.3.3 and 2.3.4 ) and the drifter o-b differences (section 2.3.2). Section 2.4 describes the implementation of the new estimates described in section 2.3 in the OSTIA system and presents the impact of the updates on the OSTIA SST analysis.

#### 2.1.1 Purpose of algorithm

The algorithm presented is designed to estimate the background error covariance parameters using o-b differences. New estimates of the background error covariances will change the relative weight given to an observation in the SST analysis. The area over which observation information is spread in the SST assimilation will also change due to the updates to the background error variances and correlation length scales. These changes should result in a more realistic SST analysis which will provide a better representation of the true ocean state on the analysis day.

The estimated parameters of the background error covariances are also used in the OSTIA system to estimate the error in the SST analysis using the analysis quality (AQ) OI

technique, see [RD.213] and the references therein. The impacts detailed above should also lead to a better estimation of this SST analysis error. The background error variances (along with the observation error variances) are also used in a Bayesian background check [RD.213], to quality control observations used in the SST analysis. Updating the background error variances should improve this background check.

## 2.2 Algorithm Description for deriving new background covariances

### 2.2.1 Algorithm Overview

A theoretical description of the algorithm is provided in section 2.2.2 whilst the steps undertaken to perform the calculations are detailed in the processing outline in section 2.2.3.

### 2.2.2 Theoretical Description

The Hollingsworth and Lonnerberg technique [RD.278] estimates the background error covariances from the spatial correlations in the observation-minus-background (o-b) differences. The method assumes that observation errors are spatially uncorrelated so correlations in the o-b differences can be attributed to correlations in the background errors.

The Hollingsworth and Lonnerberg technique detailed in section 2.2.3 estimates the background error variance within a grid box by extrapolating the o-b covariances back to zero separation distance. The total o-b variance within each grid box can be calculated directly from the o-b differences, this total o-b variance will be comprised of both the background error variance plus the observation error variance, and we assume that background and observation errors are uncorrelated. Thus having estimated the background error variance the observation error variance can also be estimated.

The Hollingsworth and Lonnerberg technique requires the observations used in the estimation to be unbiased. To this end observations from the OSTIA reanalysis v1.0 from drifting buoy and the AATSR satellite, which have both been shown to be of high quality, were used in the calculations presented here. Another requirement for the technique to give meaningful results is that the spatial coverage of the observations is good. This is the case for the satellite observations and the drifter network is deemed sufficiently mature to provide global coverage by 2002.

### 2.2.3 Processing Outline

The Hollingsworth and Lonnerberg technique estimates the background error covariances from the spatial correlations in the o-b differences. Output from the OSTIA reanalysis v1.0 [RD.213] was used in the estimates presented here.

O-b differences were calculated by bi-linearly interpolating the OSTIA reanalysis v1.0 background field to the observation location. To reduce the resources required in the estimation of the covariances the AATSR observation-minus-background differences (which are at the 1km observational resolution) were super-obbed using a median method with a radius of 6km.

The correlation calculation described below is carried out on a 1° regular grid. The following steps are carried out:

- 19 bins of separation distance are defined (in km) as follows: [10, 15, 20, 50, 100, 150, 200, 250, 300, 350, 400, 450, 500, 600, 700, 800, 900, 1000].
- Within each grid square the covariance of each o-b difference with all other o-b differences within each of the predefined separation distance bins is calculated.



These covariances are combined to give a covariance for observations in each grid square with all observations within each of the separation distances of it.

- For the anisotropic calculation (section 2.3.4) only observations within an angle of  $\pi/2$  in the North or South direction are used in the calculation of the North-South (NS) Correlations. Similarly for the East-West (EW) correlations.
- For each grid square the number of values, the mean and root mean square error of observations is output together with the covariances and number of observations contributing to the covariance for each of the separation bins. This is done for each day.
- Daily files are then combined into a single file which allows seasonal, monthly or annual covariances to be calculated as well as correlations for the whole run.

These files then undergo a further level of processing which estimates the background error variances and the correlation length scales for each of the two components of the background error covariances for each of the  $1^\circ$  grid boxes.

- The o-b covariances are regressed against separation distance for each of the  $1^\circ$  grid boxes and two Second Order Auto-Regressive (SOAR) function (equation 2.1) are combined to fit the data for each grid box. One SOAR function represents the error correlation due to mesoscale ocean features whilst the other represents the error correlations due to larger scale atmospheric synoptic conditions.

$$f(X) = V_m*(1+X/L_m)*exp(-X/L_m) + V_s * (1+X/L_s)*exp(-X/L_s) \quad (2.1)$$

where  $V_m$  and  $V_s$  are the mesoscale and synoptic scale background error variances,  $L_m$  and  $L_s$  are the mesoscale and synoptic background error correlation length scales.

- The fitting routine fits both the background error variances and the correlation length scales for both components of the background error. These are output to a file, along with the total background error variance (which is a combination of both the mesoscale and the synoptic scale components), the observation error variance and the chi-squared fit of the function to the data for each grid. See figure 2.1 for an example of the fit for a specific grid box.

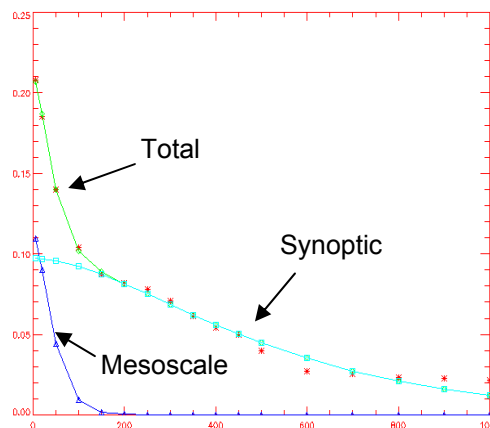


Figure 2.1. Example of the partitioning into mesoscale and synoptic scale error components of the SOAR function fitting code to the correlations regressed against separation distance.

## 2.3 Results

Results from the Hollingsworth and Lonnerberg parameter estimation are presented in the following section. Estimates using the AATSR o-b differences are presented in section 2.3.1 and section 2.3.2 provides the results from the drifting buoy o-b calculations. Section 2.3.3 investigates the seasonal variability in the estimates and section 2.3.4 looks at anisotropy in the background error covariances.

### 2.3.1 AATSR observation-minus-background results

The background error estimation calculations were carried out for the ATSR-2 and AATSR o-b differences from the OSTIA reanalysis v1.0 for 2002-2007. Calculations were also performed for the AATSR o-b differences only for the period when they were available from July 2002 to December 2007, results (not shown) were very similar to those presented below and to make the seasonal estimates more robust the 6 full years were used. The mesoscale error variances estimated from the AATSR o-b differences are shown in figure 2.2(a); spatial coverage is good with full global coverage almost being achieved. The observational coverage at high latitudes in the marginal ice zone in both hemispheres is good and increased error variances can be observed in the Northern Hemisphere marginal ice zone in figure 2.2(a). Areas of increased mesoscale error variance can be discerned in ocean regions with high SST gradients such as the Gulf Stream, Kuroshio current region, the Agulhas retroflexion and the Zapiola Rise region off the coast of Argentina.

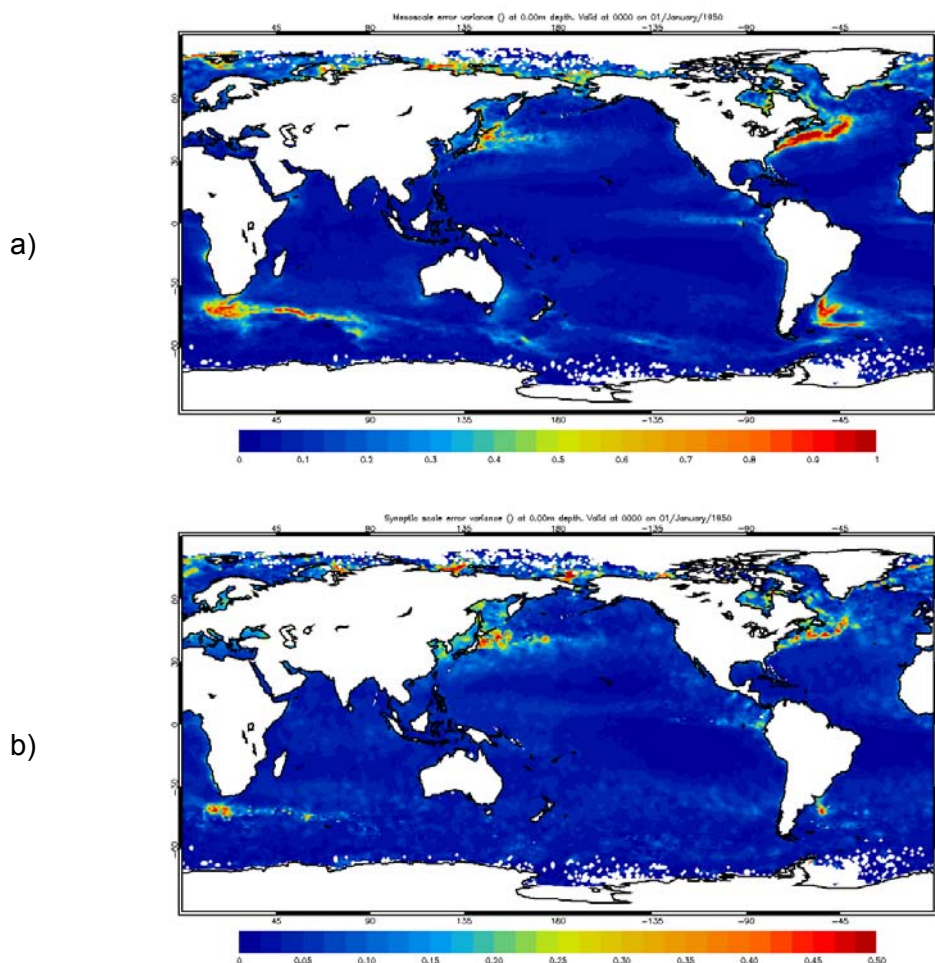


Figure 2.2. Mesoscale (a) and synoptic scale (b) background error variances estimated from the AATSR o-b output. (Note different scale on (a) and (b).)

Despite the super-obbing applied to the AATSR o-b data, see section 2.2.2, the resolution of the error variances is still adequate to represent small ocean scale features such as heightened variances in the Eastern Tropical Pacific due to upwelling caused by Tehuano, Papagayo and Panama wind events in central America as observed in figure 2.2(a).

Figure 2.2(b) shows the synoptic scale error variances for the AATSR estimates, the magnitude of the synoptic component is reduced compared to the mesoscale component of the background error variance, note the different scales in figures 2.2(a) and (b). Areas of increased variance in the synoptic scale are found in the high SST gradient regions described above where the mesoscale variance was also magnified, see figure 2.2(a). This may indicate a problem with the decomposition of the variances into mesoscale and synoptic scale components, some of the mesoscale variability may be contaminating the synoptic scale error variances. However these regions of enhanced mesoscale ocean variability are also regions of enhanced synoptic activity so the similar spatial patterns might be expected to a certain extent. There is a question mark on the validity of the assumption made of observation errors being spatially uncorrelated, and a major component of the spatial correlations in the observation error would be due to atmospheric conditions. These errors would have length scales close to those of synoptic systems and such correlations would show up in the synoptic component of the background error partitioning employed here. It is therefore possible that part of the synoptic scale background error variance may be due to contamination by correlated observation error. This possibility is investigated further in section 2.3.2 using the drifting buoy estimates.

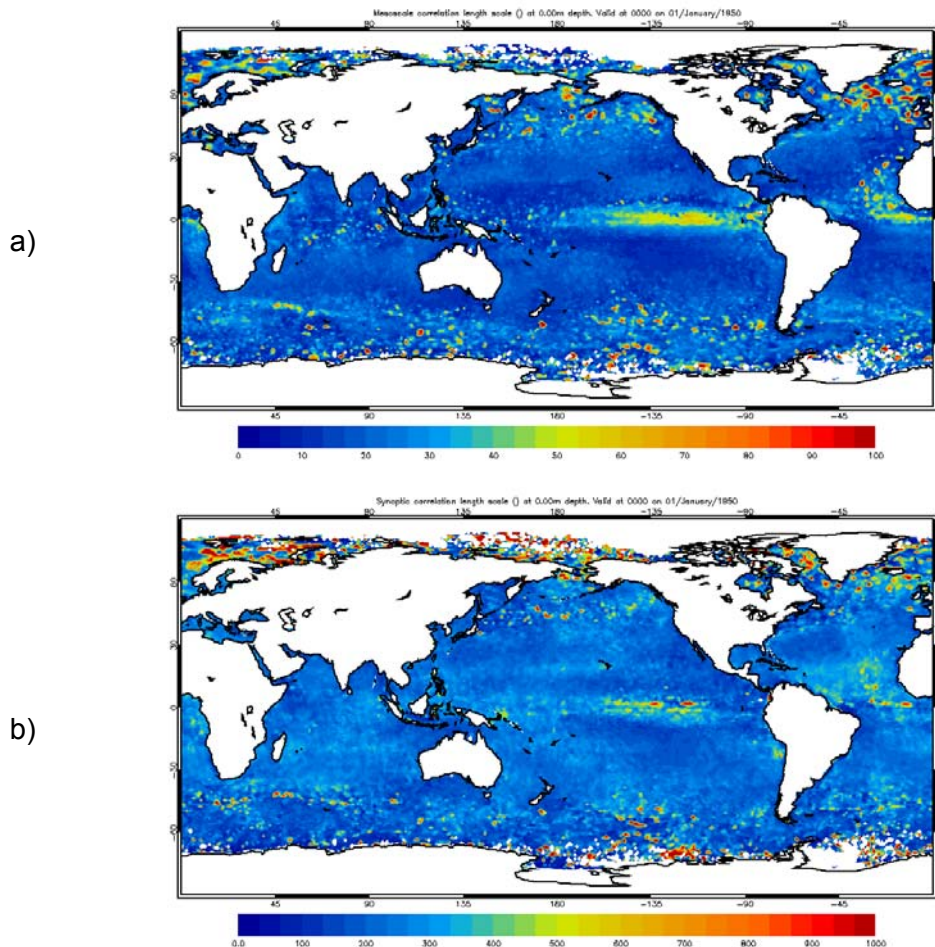
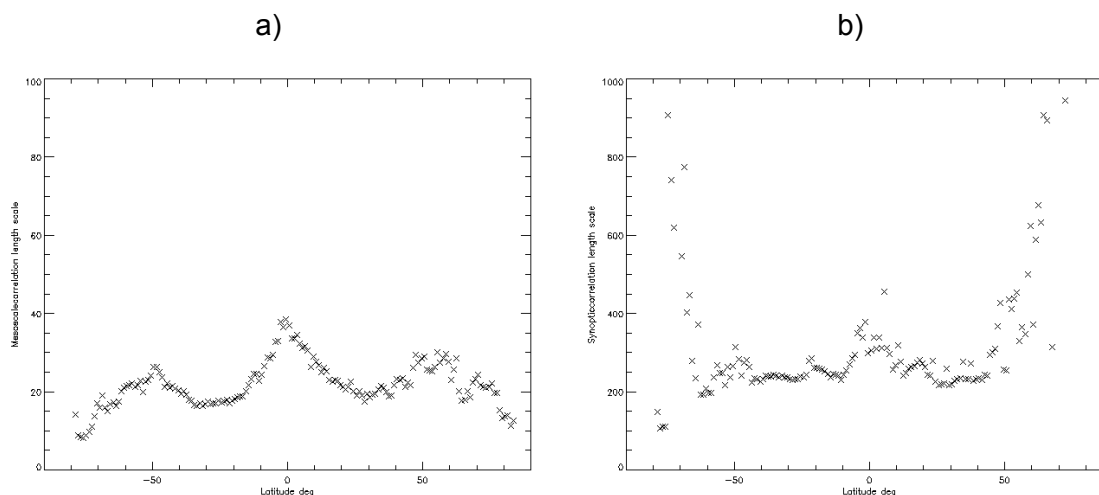


Figure 2.3. Mesoscale (a) and synoptic scale (b) correlation length scales (km) estimated from the AATSR o-b output. (Note different scale on (a) and (b).)



**Figure 2.4. Zonally averaged mesoscale (a) and synoptic scale (b) correlation length scales (km) estimated from the AATSR o-b output. (Note different scale on (a) and (b).)**

Figure 2.3 shows a spatial map of the mesoscale and synoptic scale correlation length scales for the AATSR estimates. Figure 2.3(a) illustrates that the mesoscale correlation length scales are lengthened towards the equator, this lengthening can be discerned in the Eastern Tropical Pacific and in the Tropical Atlantic. A lengthening of the correlation length scale also occurs at mid-latitudes of between approximately 30°-60° in the Northern and Southern Hemispheres and can be seen in the North Atlantic and Pacific and in the Southern Ocean, this is probably due to enhanced synoptic activity in the temperate regions. Figure 2.4(a) shows the zonal average of the mesoscale length scale in 1° zonal bands, and nicely illustrates the lengthening at mid-latitudes to a zonal average of approximately 27 km and the lengthening at the equator to approximately 40 km. Outside of these regions in the ocean gyres, figures 2.3(a) and 2.4(a) show that the length scales are relatively stable at around 20 km. At high latitudes spatially noisy long length scales can be observed in figure 2.3(a).

The lengthening of the synoptic correlation length scales in the Tropical Pacific and Atlantic can be observed in figure 2.3(b). The synoptic scale zonal averages, shown in figure 2.4(b) increase from approximately 240 km to approximately 350 km at the equator. Figure 2.3(b) also shows that the lengthening at mid-latitudes in the Northern and Southern Hemispheres described previously for the mesoscale length scales is also apparent in the synoptic length scales. The zonal average is increased from 240 km to approximately 300 km. The noise at high latitudes is larger than that observed for the mesoscale component of the errors and tends to be observed in the marginal ice zone in figure 2.3(b) and contaminates the zonal averages in figure 2.4(b).

### 2.3.2 Drifter observation-minus-background results

The background error estimation calculations were also carried out for the drifting buoy o-b differences from the OSTIA reanalysis v1.0 for 2002-2007. The mesoscale error variances estimated are shown in figure 2.5; the sparsity of the drifter network is highlighted by the large gaps in the variance field. These gaps occur where there are not enough observational coverage for the Hollingsworth and Lonnberg and function fitting

technique to work, and can be discerned in tropical regions and at mid-latitudes in the Pacific and Atlantic. There are also gaps at High Latitudes compared to the AATSR estimates shown in figure 2.2(a) due to few drifter observations being available in the marginal ice zone in both hemispheres. Using the other in situ observational types in the calculation, which are moored buoys and ship observations, did not fill these gaps.

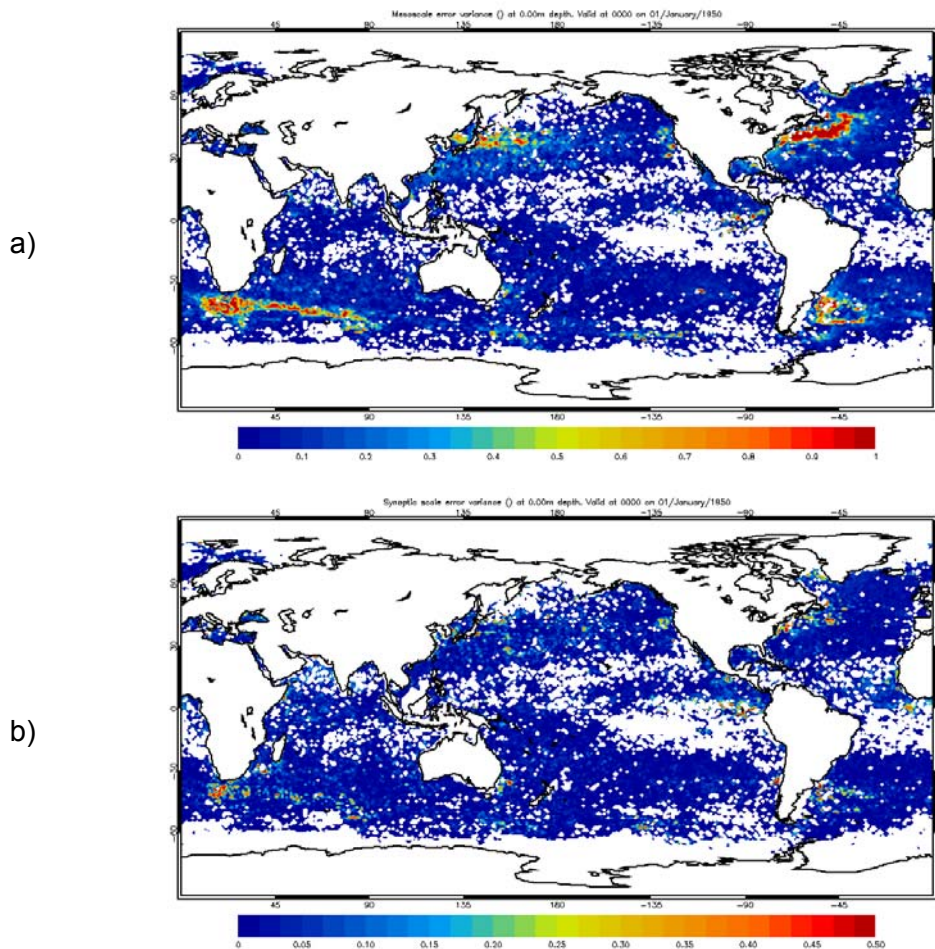


**Figure 2.5. Mesoscale (a) and synoptic scale (b) background error variances estimated from the drifting buoy o-b output. (Note different scale on (a) and (b).)**

Figure 2.5(a) shows that the mesoscale error variance is again increased in regions of high SST gradients similar to the AATSR estimates as shown in figure 2.2(a). Figure 2.5(b) shows the synoptic scale error variance to again be decreased compared to the mesoscale variance. The synoptic variance tends to be noisier spatially but patterns of increased variance are again found in the high SST gradient regions described above where the mesoscale variance was also magnified. Comparison with the AATSR estimates shows that the drifter synoptic variance estimates are noisier than those shown in figure 2.2(b) but the general pattern of enhanced variances in high gradient regions is similar, indicating possible mesoscale error contamination.

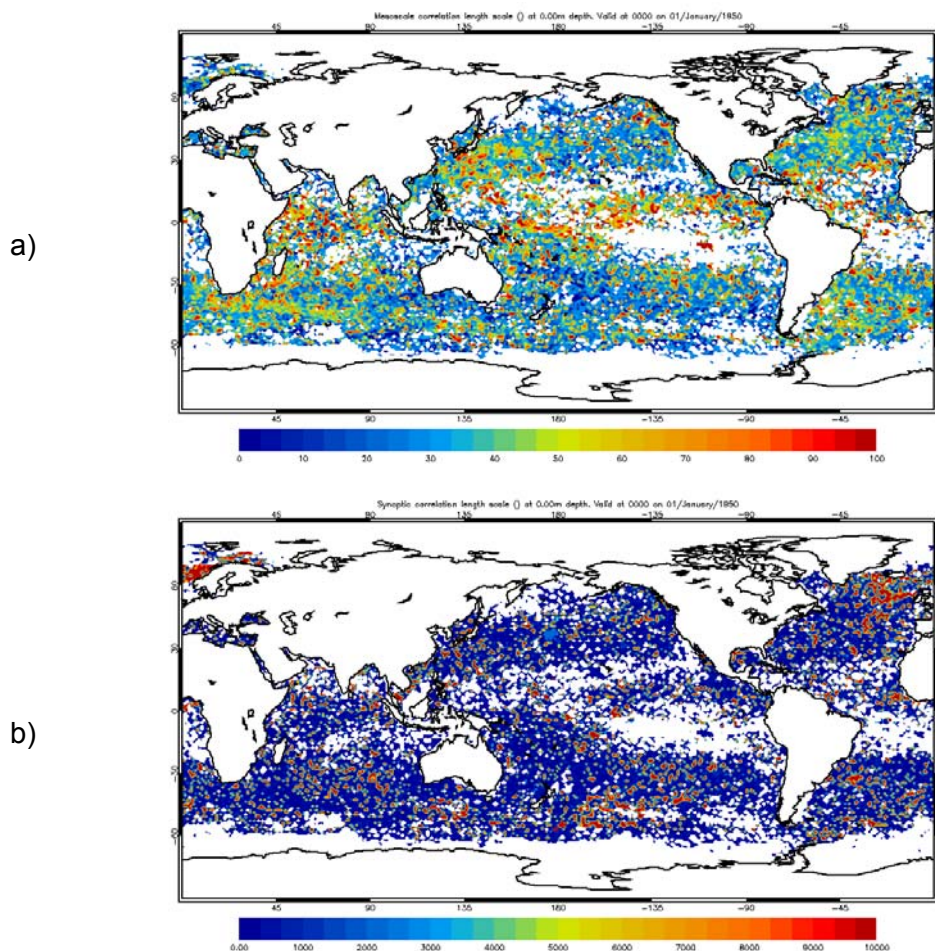


**Figure 2.6. Mesoscale (a) and synoptic scale (b) correlation length scales (km) estimated from the drifting buoy o-b output. (Note different scale on (a) and (b).)**

Figure 2.6 shows a global map of the mesoscale (a) and synoptic scale (b) correlation length scales estimated from the drifter o-b data. The mesoscale correlation length scales are lengthened towards the equator. The zonal average of the length scale (not shown) increases relatively smoothly from 25 km at high latitudes to 55 km at the equator. The increase seen in figure 2.6(a) is less zonally confined than the increase seen in the AATSR mesoscale length scales shown in figure 2.3(a), which outside of the tropics and the temperate synoptic regions was relatively more consistent.

The synoptic scales, shown in figure 2.6(b), appear spatially noisy and the length scales are excessively long, with the average scale being 2280 km. This is due to a problem with the function fitting routine (see section 2.2.3). The partitioning of the covariance into mesoscale and synoptic scale components has failed in these cases, the synoptic component fit is a flat line which has very small variance and a very long length scale. This is likely due to insufficient observational coverage for the function fitting procedure and the partitioning to work correctly.

Despite these shortcomings, the parameter estimates from the drifter o-b data provide a valuable sanity check on the AATSR estimates. The spatial patterns of the mesoscale and synoptic scale variances are similar for estimates made using both observation types. This is of particular relevance for the synoptic scale variances where there is the possibility of correlations in the observation error contaminating the AATSR synoptic

background error estimates (as discussed in section 2.3.1). The observational errors in the drifting buoy data should not be associated with atmospheric synoptic conditions. As these results agree with the AATSR results, contamination of the AATSR synoptic background errors by observational errors is unlikely. The similarity between the synoptic scale variances provides a degree of confidence in the AATSR synoptic scale variance estimates.

### 2.3.3 AATSR Seasonal observation-minus-background results

The better observational coverage of the AATSR estimates discussed in section 2.3.1 means that seasonal estimates of the covariance parameters can be made. Figure 2.7 and 2.8 show mesoscale and synoptic scale error variances respectively for DJF (December, January, February) and JJA (June, July, August). The improved spatial coverage at high latitudes in the Summer Hemisphere can be observed in figures 2.7(a) and (b) due to the retreat of the sea ice. As described previously the mesoscale variances in the marginal ice zone in the Northern Hemisphere are increased. The increased variances due to upwelling caused by the Central American wind events described previously are shown to be seasonally variable and are strongest during the Northern Hemisphere Winter.

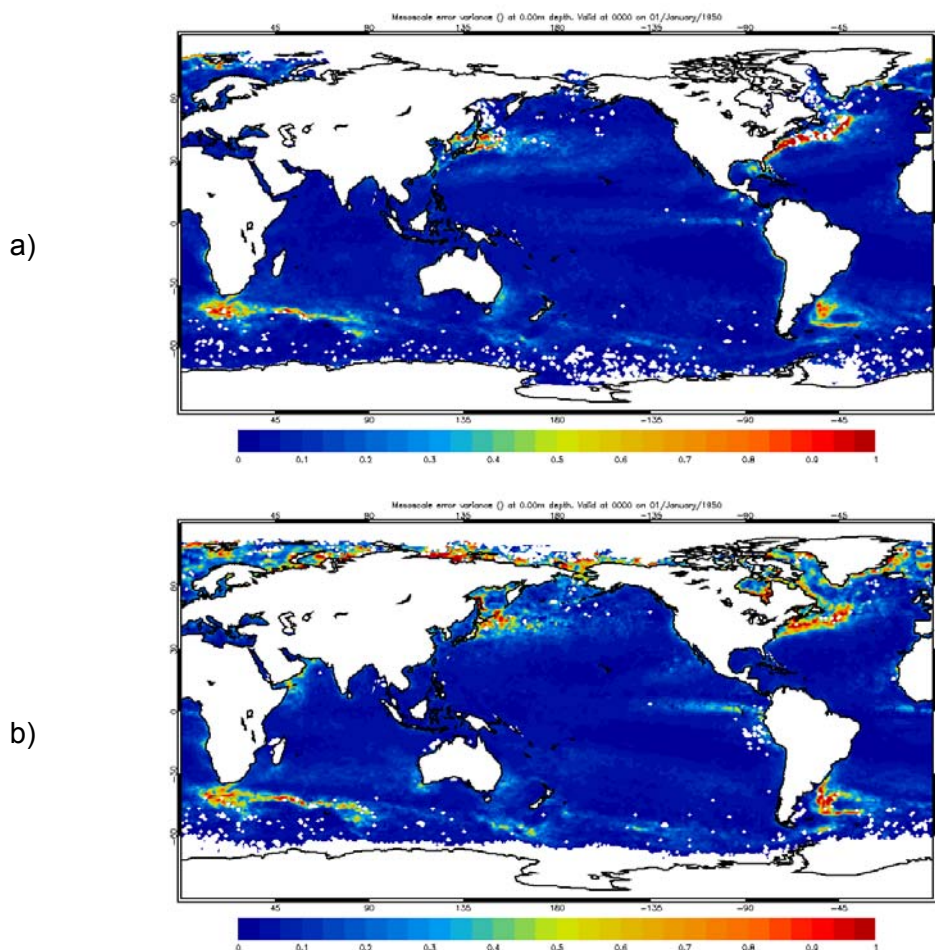
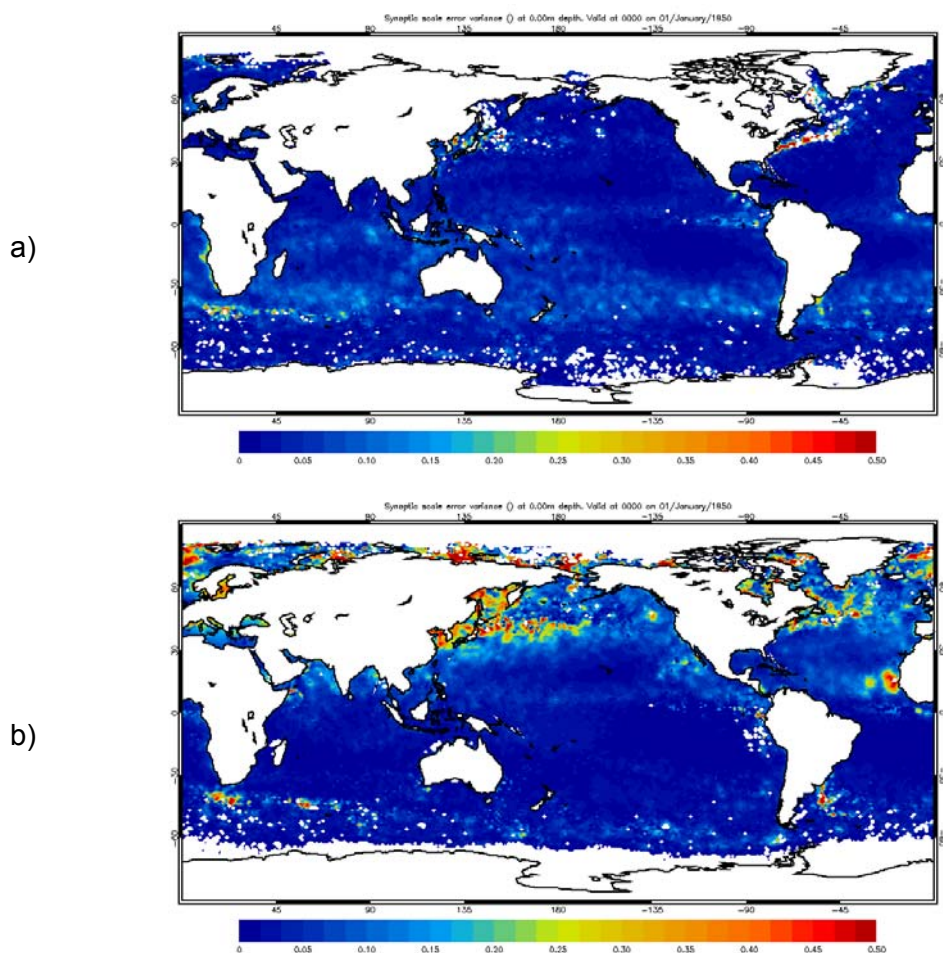


Figure 2.7. Seasonal mesoscale background error variances for (a) DJF and (b) JJA estimated from the AATSR o-b output.



**Figure 2.8. Seasonal synoptic scale background error variances for (a) DJF and (b) JJA estimated from the AATSR o-b output.**

The synoptic variances show a distinct seasonal cycle with increased error variance occurring in the Summer Hemisphere at mid-latitudes, figure 2.8. This seasonal variability could be caused by contamination by a diurnal warming signal in the analysis during the summer which would be expected to occur on the scale of synoptic systems. Spatial variability, which would also occur on the scale of synoptic systems, in the cool-skin effect could also affect the AATSR estimates. The AATSR skin SST measurement is corrected to a bulk SST within the OSTIA system using a constant value of 0.17 K [RD.213], which doesn't account for these small scale variations. The seasonal cycle manifests itself in the magnified variances in JJA in the Kuroshio current region compared to the DJF estimates. Enhanced synoptic scale variability also occurs in JJA in the Western Pacific due to the Asian Monsoon which can be discerned in 2.8(a). A region of increased variability can also be observed in the Tropical Atlantic off the North West African coast in JJA, where seasonally enhanced tropical storm activity occurs. Figure 2.8(b) illustrates that increased synoptic scale variability in the Indian Ocean can be observed in JJA associated with the Indian Monsoon, the same increased variability can also be discerned to lesser extent in the mesoscale variances.

Seasonal estimates of the correlation length scales for both components were calculated, the mesoscale correlation length scales (not shown) show little significant seasonal variability. Some seasonal variability was found in the synoptic length scales (not shown). The lengthening of the AATSR synoptic length scale discussed previously in section 2.3.1 in the Tropics is larger in JJA compared to DJF. There is also a lengthening in the Indian Ocean in JJA due to the Indian Monsoon.



### 2.3.4 AATSR anisotropic observation-minus-background results

To look at anisotropy in the correlation length scales the estimation procedure was carried out using correlations in the East-West and in the North-South direction separately, see section 2.2.3. As the variances are estimated by extrapolating the correlations back to zero separation distance it is expected that the EW and NS estimates of the background error variances (not shown) will be similar, this was found to be the case.

The lengthening of the mesoscale correlation length scale towards the equator described previously can be observed in figures 2.9(a) and (b) in both the EW and NS directional estimates. Comparison of the EW and NS length scales shows spatial differences in the directional estimates. The lengthening occurs in the EW direction in the Eastern Tropical Pacific, whilst the lengthening in the NS direction occurs in the Western Tropical Pacific and in the Indian Ocean. The lengthening in the Tropical Atlantic occurs in both directions as does the lengthening at mid-latitudes discussed previously. Figure 2.10 shows the zonal averages of the anisotropic correlation length scales. The mesoscale length scale is lengthened at the equator from approximately 17 km to approximately 38 km for the EW estimates and from approximately 20 km to approximately 43 km for the NS estimates. These global zonal averages were found to be relatively robust when calculated across different ocean regions. The scales lengthen at mid-latitudes to approximately 27 km for the EW and NS estimates.

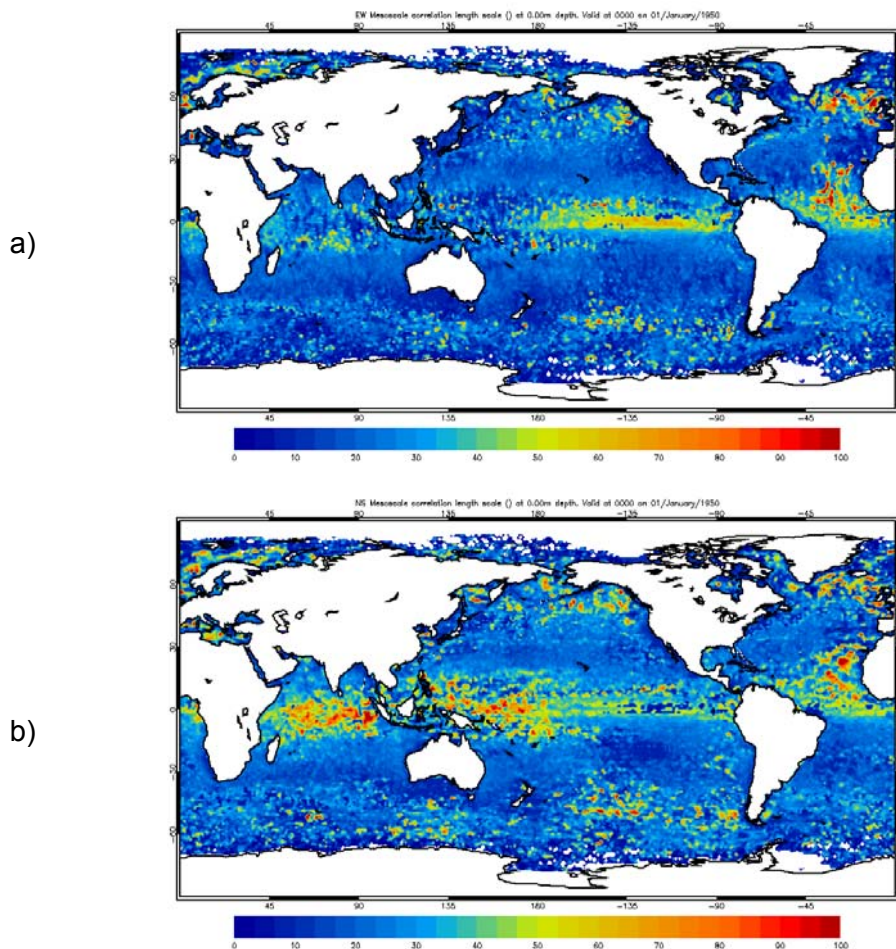
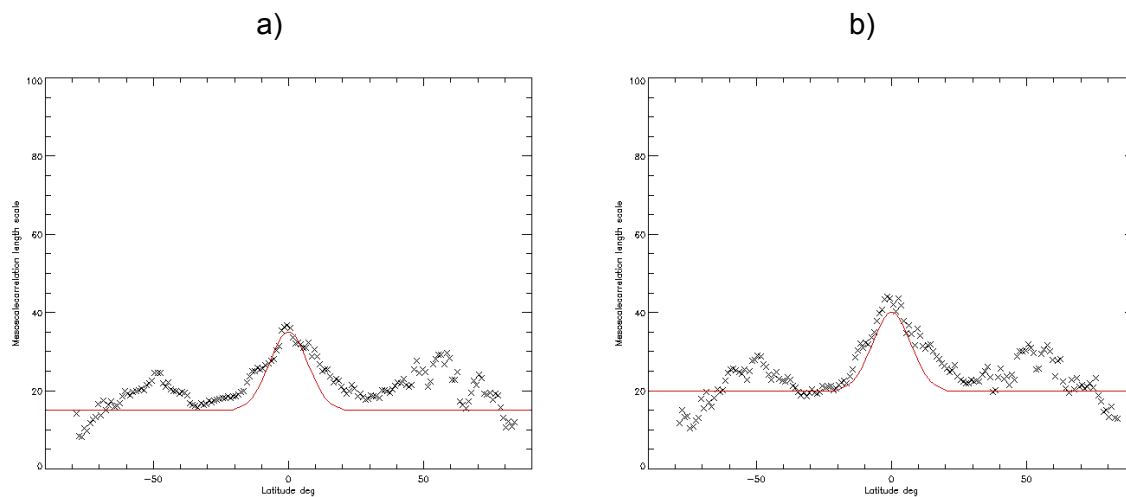


Figure 2.9. Mesoscale correlation length scales (km) in the (a) East-West and (b) North-South direction estimated from the AATSR o-b output.



**Figure 2.10. Zonal averages of the mesoscale correlation length scales (km) in the (a) East-West and (b) North-South direction estimated from the AATSR o-b output. Parameterisations described in section 2.4 are shown in red.**

The unidirectional synoptic correlation length scales are shown in Figure 2.11. The equatorial lengthening of the length scale occurs in both the EW and NS directions and can be observed in the Eastern Tropical Pacific and in the Tropical Atlantic. A lengthening in the NS direction can also be observed in the Eastern Tropical Pacific and in the Indian Ocean. The lengthening at mid-latitudes described for the all directional estimates can be discerned in both the EW and NS directions. As in figure 2.3(b) for the all-directional estimates the E-W and N-S synoptic length scales tend to be spatially noisy at high latitudes. Figure 2.12 shows that the zonal average synoptic length scale increases from 210 km to 350 km in the EW direction and from 260 km to 550 km in the NS direction. The magnitude of the E-W and N-S directional mid-latitude lengthening is similar to that observed at the equator.

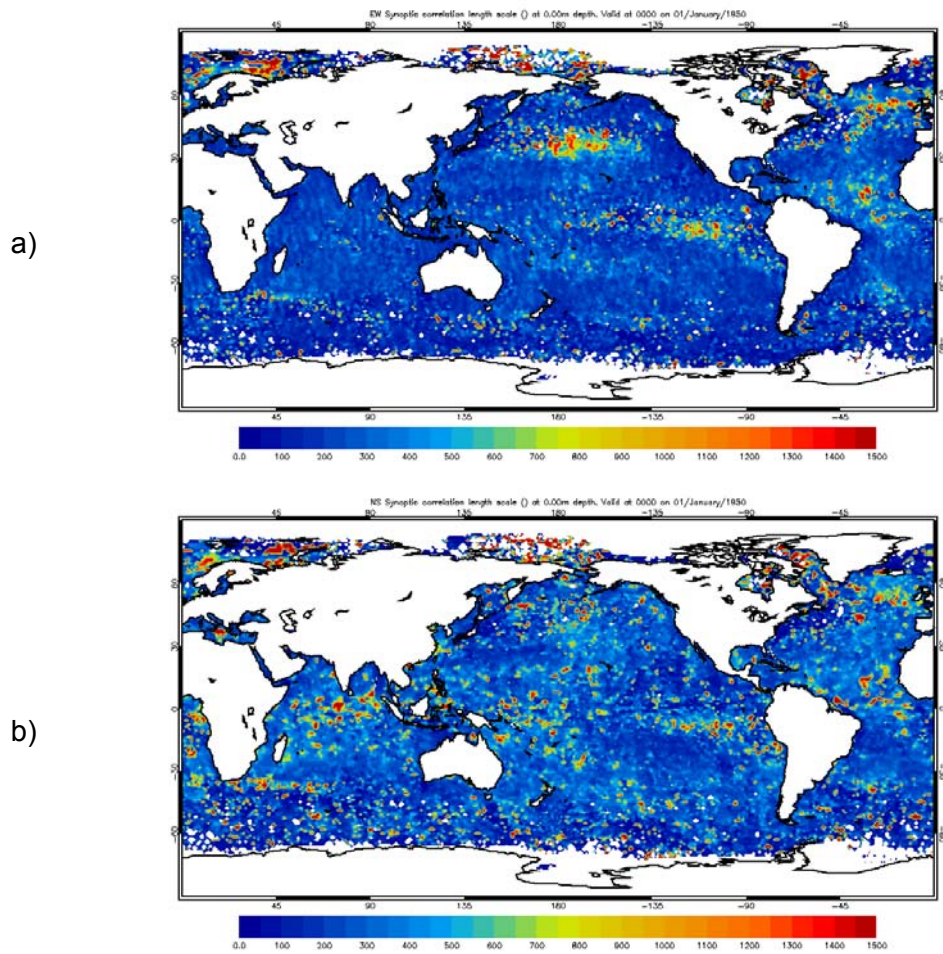


Figure 2.11. Synoptic correlation length scales (km) in the (a) East-West and (b) North-South direction estimated from the AATSR o-b output.

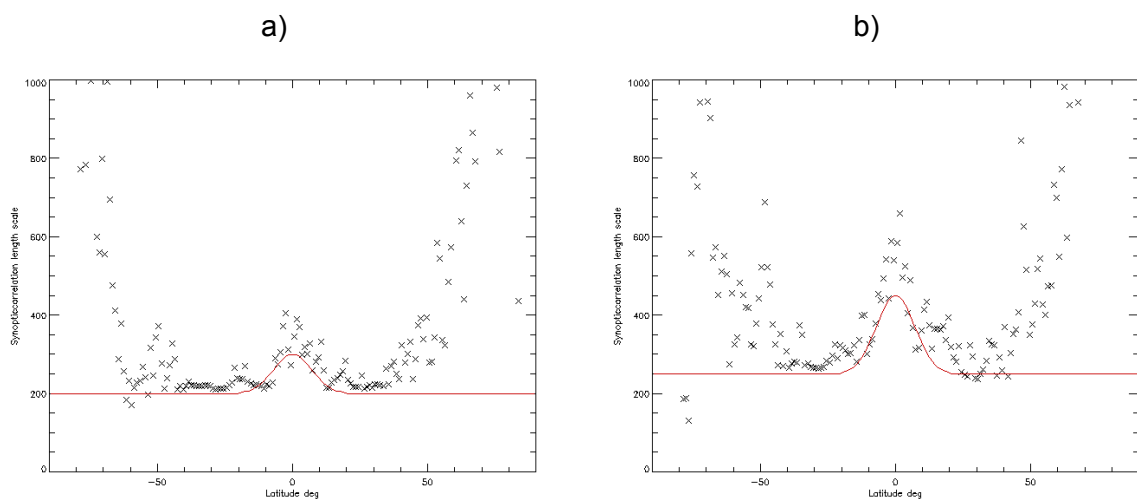


Figure 2.12. Zonal averages of the synoptic correlation length scales (km) in the (a) East-West and (b) North-South direction estimated from the AATSR o-b output. Parameterisations described in section 2.4 are shown in red.

## 2.4 Implementation

The estimated background error covariance parameters described in section 2.3 were implemented in the OSTIA system to test the impact of the updates on the OSTIA SST analysis. Global spatial maps of seasonally varying mesoscale and synoptic scale background error variances estimated using the AATSR o-b data were implemented. These replace the temporally static two component error variances which were estimated from a 2 year model hindcast (RD.279).

The current OSTIA assimilation code [RD.213] does not currently allow global spatial maps of the two correlation length scale components to be directly used in the assimilation. It is desirable to use both the zonal variability shown in figures 2.4, 2.10 and 2.12 and the anisotropy in length scales discerned in the E-W and N-S calculations in the SST assimilation. The global zonal averages shown in figures 2.10 and 2.12 were found to be relatively robust across different ocean basins (not shown). Thus anisotropic length scales were parameterised to be globally latitudinally varying using the following functional form,

$$L = L_c + A \exp^{-T^2} \left( \text{for } | \text{Latitude} | \leq 20^\circ \right)$$

$$T = \frac{\text{Latitude}}{S}$$

$$L = L_c \left( \text{for } | \text{Latitude} | > 20^\circ \right)$$

Where  $L$  is the final length scale (used for  $L_m$  or  $L_s$  in equation 2.1),  $L_c$  is constant length scale,  $A$  and  $S$  are amplitude and scale parameters respectively.

The anisotropy observed in the correlation length scales implies that parameter values differ between the E-W and N-S length scales as well as between the mesoscale and synoptic length scale. The parameter values used are shown in table 2.1. The parameterisations are shown as the red lines in figures 2.10 and 2.12. These anisotropic latitudinally varying length scales replace static length scales of 10 km for the mesoscale component and 100 km for the synoptic scale, which are currently used in OSTIA.

Scale	Direction	Lc	A	S
Mesoscale	EW	15 km	20 km	10
Mesoscale	NS	20 km	20 km	10
Synoptic scale	EW	200 km	100 km	10
Synoptic scale	NS	250 km	200 km	10

**Table 2.1 Parameter values for the latitudinally varying correlation length scales.**

In the operational NRT OSTIA and OSTIA reanalysis systems the OI equation is solved using an iterative approach where the number of analysis iterations is set to be 10. If the assimilation scheme does not converge to the optimal solution after 10 iterations, the SST analysis can appear too smooth, as the scheme will fit the large scale features first and so small scale ocean features are not resolved. Recent experiments using pseudo-observations showed that increasing the number of assimilation iterations resulted in improvements in the feature resolution of the analysis without introducing observational noise through overfitting the data. Within this body of work it was decided to further investigate the impact of increasing the number of analysis iterations.

To test the impact of these updates a series of twin experiments was carried out for a 1 month run of the NRT OSTIA system in March 2012, which uses satellite and in-situ data as specified in [RD.213]. To validate the impact of the new background error estimates on the accuracy of the OSTIA SST, analysis assimilated observation-minus-background statistics have been used. In the NRT OSTIA system an assimilation window of 36 hrs is used. The majority of observations used in the o-b validation will therefore be different to those assimilated into the background field. These observations thus provide a pseudo-independent validation set, which is further discussed in [RD.213]. Table 2.2 lists the experimental configurations that were tested, which includes a test to assess the impact of withholding in-situ data.

	No. of iterations	Length scales	Variiances	Using in-situ data?
Control	10	10 km 100km	Old	Yes
Both 10 its	10	Latitudinally varying	New	Yes
Var 10 its	10	10 km 100km	New	Yes
Both 100 its	100	Latitudinally varying	New	Yes
Var 100 its	100	10 km 100km	New	Yes
No in-situ	100	Latitudinally varying	New	No

**Table 2.2 OSTIA experiment configurations to test the impact of the new background error estimates on the SST analysis.**

Table 2.3 shows the o-b statistics averaged over the 1 month trial period combined globally and in ocean regions for each of the trial experiments for the drifting buoy observations. See [RD.213] for a description of the o-b calculation procedure. When the analysis scheme is run with 10 iterations using the new background error estimates, the global root mean square error (RMSE ) reduces from 0.52 K to 0.45 K for the drifting buoy statistics. A greater improvement is seen when only the new variiances are used in conjunction with the old correlation length scales where the global o-b RMSE decreases from 0.52 K to 0.39 K. When the assimilation scheme is run with 100 iterations the improvement in accuracy is even more marked with an RMSE of 0.37 K for both the new variance and length scale estimates and 0.35 K for the new variance estimates only. A similar decrease in RMSE is seen across most ocean regions despite the regional accuracy being spatially variable due to differences in the atmospheric and oceanographic characteristics between regions. The mean o-b bias shows little change between the different experiments globally and in most regions; differences occur in regions where the SST analysis has a large mean bias due to limited number of observations such as the Arctic, Mediterranean and the European North-West shelf.

	Control		Both 10 its		Var 10 its		Both 100 its		Var 100 its	
	RMSE	Bias	RMSE	Bias	RMSE	Bias	RMSE	Bias	RMSE	Bias
Global Ocean	0.52	-0.01	0.45	-0.01	0.39	0.00	0.37	0.00	0.35	0.00
Arctic	0.58	0.14	0.57	0.21	0.47	0.14	0.45	0.12	0.41	0.12
North West Shelf	0.40	0.17	0.46	0.21	0.40	0.17	0.39	0.17	0.34	0.15
Mediterranean	0.56	0.33	0.46	0.27	0.47	0.28	0.48	0.28	0.47	0.28
North Atlantic	0.62	0.04	0.51	0.04	0.44	0.04	0.42	0.04	0.40	0.04
Tropical Atlantic	0.40	-0.02	0.40	-0.07	0.36	-0.03	0.35	-0.03	0.31	-0.01
South Atlantic	0.48	0.02	0.44	0.00	0.38	-0.02	0.35	-0.02	0.33	-0.02
North Pacific	0.54	0.03	0.46	-0.01	0.40	-0.01	0.38	-0.01	0.35	-0.01
Tropical Pacific	0.35	0.00	0.31	-0.03	0.28	0.00	0.28	-0.01	0.27	-0.01
South Pacific	0.39	-0.02	0.37	-0.06	0.32	-0.04	0.30	-0.04	0.28	-0.03
Indian Ocean	0.46	-0.02	0.42	-0.04	0.38	-0.03	0.36	-0.03	0.33	-0.01
Southern Ocean	0.48	0.01	0.46	-0.02	0.39	-0.01	0.35	-0.01	0.34	0.00

**Table 2.3 Global and regional statistics of the drifter observation-minus-background RMSE and mean bias averaged over March 2012 for the different OSTIA experimental configurations (in K).**

	Control		Both 10 its		Var 10 its		Both 100 its		Var 100 its		No insitu	
	RMSE	Bias	RMSE	Bias	RMSE	Bias	RMSE	Bias	RMSE	Bias	RMSE	Bias
Global Ocean	0.45	0.04	0.42	0.03	0.38	0.03	0.37	0.03	0.36	0.04	0.40	0.05

**Table 2.4 Global statistics of the AATSR observation-minus-background RMSE and mean bias averaged over March 2012 for the different OSTIA experimental configurations (in K).**

	Control		Both 10 its		Var 10 its		Both 100 its		Var 100 its		No insitu	
	RMSE	Bias	RMSE	Bias	RMSE	Bias	RMSE	Bias	RMSE	Bias	RMSE	Bias
Global Ocean	0.47	0.03	0.52	0.03	0.47	0.04	0.43	0.04	0.42	0.05	0.44	0.04

**Table 2.5 Global statistics of the top level ARGO observation-minus-analysis standard deviation error and mean bias averaged over March 2012 for the different OSTIA experimental configurations (in K).**

The AATSR o-b statistics show similar decrease in RMSE to the drifter statistics as shown in table 2.4 but the magnitude of the improvement is slightly less. Using both the new variance and length scale estimates the global RMSE decreases from 0.45 K to 0.42K and 0.37 K for the 10 and 100 iteration runs respectively. For the new variance only run the global RMSE decreased from 0.45 K to 0.38 K and 0.36 K for the 10 and 100 iteration runs respectively. Once more this increase is seen across most ocean regions (not shown). The mean bias remains relatively unchanged across the different experiments.

Independent validation of the impact of the new error estimates on the accuracy of the OSTIA analysis was carried out via comparison with top-level ARGO data (between 3-5m

depth) which have been shown to be a good measure of foundation SST via three way comparisons with drifting buoy and AATSR data (Merchant and Corlett, pers. comm.). ARGO observations of between 3 and 5 m were obtained from the EN3 data base which had undergone a series of QC checks [RD.282]. The OSTIA SST was bi-linearly interpolated to the ARGO observation location and the difference calculated. Statistics were then calculated globally and in different ocean regions; global results are show in table 2.5 . Using 10 analysis iterations the global standard deviation error is increased from 0.47 K to 0.52 K using both the new variance and new length scale estimates, and remains at 0.47 K using the new variance estimates only. Increasing the number of analysis iterations to 100 results in the standard deviation error decreasing further to 0.44 K for both new parameters and to 0.42 K for the new variances only.

These ARGO results are not as encouraging as the validation results obtained using assimilated data presented in tables 2.3 and 2.4. The sparsity of ARGO observations (approximately 300 observations globally daily) do not give the observational coverage to capture the changes in daily mesoscale variability that might be introduced through updating the background error covariance parameters. We would however expect the ARGO observational coverage to be sufficient to represent the regional accuracy changes. Using the new estimates with an increased number of analysis iterations does lead to a decrease in the ARGO observation-minus-analysis standard deviation error.

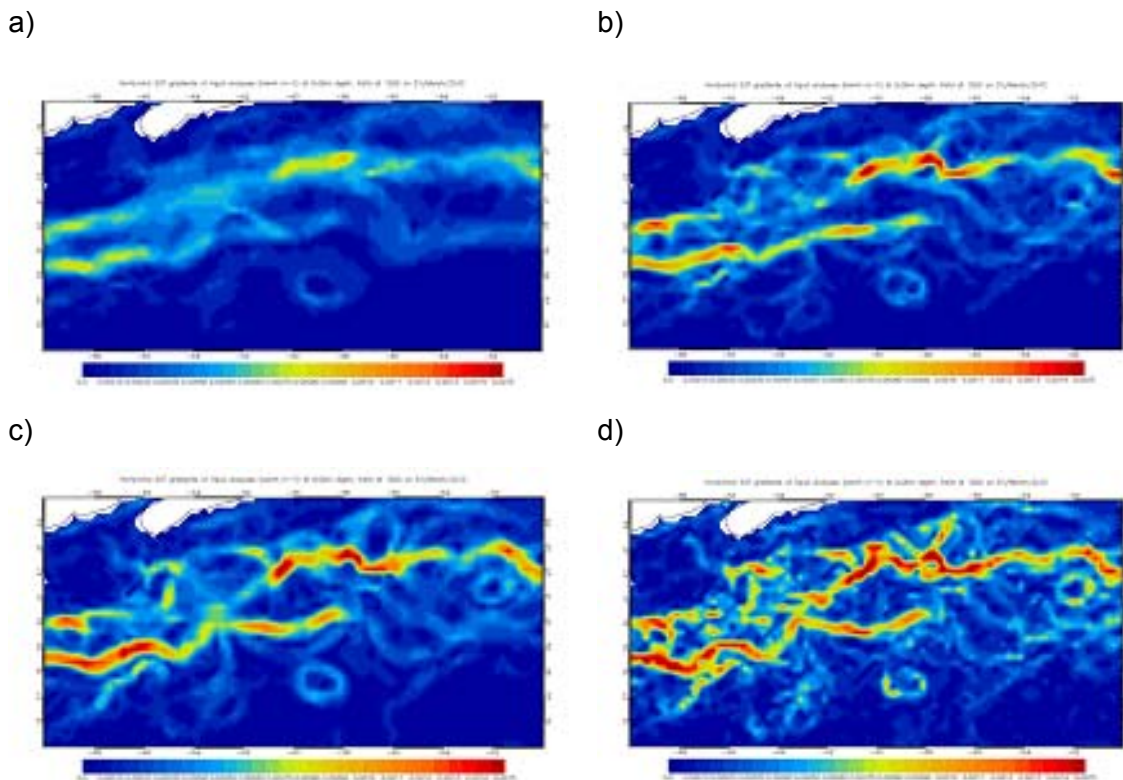


Figure 2.13. SST gradients in the Gulf Stream ( $10^*K/m$ ) for (a) Control, (b) Var 10 its, (c) Both 100 its and (d) Var 100 its . Scale ranges from 0 to 0.0015.

The statistical validation presented previously gives a measure of the large-scale accuracy improvements of the new error estimates on the OSTIA analysis. The changes to the background error variances and correlation length scales as well as the number of assimilation iterations will also affect how the OSTIA analysis resolves small scale ocean

features. To look at the impact of the error updates on the SST analysis feature resolution the daily gradients of the OSTIA SST analysis have been calculated for each of the experimental runs. Gradients are calculated in the x- and y-direction separately and then combined to give the average SST gradient on the full-resolution OSTIA grid before being interpolated to a  $\frac{1}{4}^\circ$  grid for output. Animations of these gradients were studied to investigate the feature resolution of the SST analyses and the contamination of observational noise. Figure 2.13 shows gradient fields in the Gulf Stream region for 31st March 2012, a representative day of the month long trial. The magnitude of the SST gradients is increased in the 100 iteration experiments, figures 2.13(c) and (d), compared to the Control experiment, figure 2.13(a). Figure 2.13(d) shows that the largest gradients are present in the run where the new variances only were used in conjunction with the old correlation length scales. Animating the fields showed that temporal observational noise was present in the gradient field. This is likely due to the old length scales being too short and the assimilation now fully representing these scales in the analysis (due to the increased number of iterations). The gradients represented in the run using both new variances and the new correlation length scales shown in figure 2.13(c) were more temporally consistent with realistic ocean features.

Withholding in-situ data reduced the accuracy of the analysis with respect to AATSR observations; the o-b RMSE increased from 0.37 K to 0.40 K compared to the corresponding run which used in-situ data. This increase in AATSR o-b RMSE may seem counter-intuitive as one might expect the analysis to be closer to the AATSR observations in the run without in-situ data. Due to the small swath of the instrument the AATSR observations sample a different region of the ocean on each day (near global coverage is achieved over approximately 4 days), this means that the AATSR observations assimilated into the background field will be over a different region to those we are using in the validation. The result suggests that the in-situ observations complement the AATSR observations and improve the NRT OSTIA analysis accuracy via its impact in regions yet to be observed by the AATSR instrument. The analysis accuracy compared to ARGO observations was not significantly affected, with the ARGO observation minus analysis standard deviation error increasing slightly from 0.43 K to 0.44 K. The feature resolution of the analysis without in-situ observations (not shown) was very similar to that observed for the corresponding run with the observations shown in figure 2.13(c).

Taking into account the results presented above it was decided to implement both the new background error variances and the new correlation length scales in the OSTIA system. Despite the new variances alone achieving a bigger improvement in both the assimilated o-b validation and the independent ARGO observation minus background validation, the results of investigations into the small scale feature resolution of the OSTIA analysis showed that using new estimates in both parameters in conjunction resulted in a more realistic SST analysis. The function fitting routine employed in the setup of the Hollingsworth and Lonnberg technique employed here fits both the background error variances and the correlation length scales simultaneously; this implies that the variances and the length scales go hand-in-hand which provides further justification for using both new estimates in the OSTIA implementation.

## 2.5 Assumptions and limitations

### 2.5.1 Algorithm performance

The Hollingsworth and Lonnberg estimation technique employed here makes a number of assumptions on the error characteristics of the input data. An assumption is made that the observation and the background field used in the calculations are independent. In this work, the OSTIA reanalysis v1.0 was used, which had an assimilation window of 72 hours, so observations used in the o-b differences are those within  $\pm 36$  hrs of 1200 UTC on the analysis day. Therefore, the OSTIA background field and the observations used in



the o-b calculation are not independent, furthermore the o-b field on any given day will not be independent of those on previous or subsequent days. However, during the validation of the OSTIA analysis v1.0, the lack of independence between the observations and the background field was deemed to have minimal impact on the validity of the validation results, see [RD.239] for this discussion.

It is also assumed that the observations used in the parameter estimation technique are unbiased and are not spatially correlated. The drifter and AATSR observations used here have been shown to be unbiased, [RD.239]. It might be expected though that observational errors may contain spatial correlations. For the AATSR observations a major component of the observation error may be due to errors in the atmospheric correction of the satellite retrieval which would be on the scales of atmospheric synoptic systems. Smaller scale correlations in the observational errors may also exist due to correlations along the satellite swath. The drifting buoy observation correlations would be expected between different observations from the same platform over the course of the assimilation window. It is expected that these spatial correlations for the different observation types occur at different spatial scales. Section 2.3.2 showed that estimates calculated using both observation types were similar and thus validate each other. Without knowing the spatial correlations in the observations explicitly, using different observations gives us greater confidence that the impact of violating this assumption is minimal.

The validity of partitioning the background error into those associated with mesoscale and synoptic scale variability was considered in section 2.3.1. However the impact of the updates presented here on the SST assimilation will be through the total background error variances and the effective correlation length scale, i.e. the combination of the two components. This means that the possibility of erroneous assignment of o-b variability to one or the other of the components through the function fitting will have minimal impact on the assimilation.

## 2.6 Conclusions

The new background error covariance parameters have been presented which were derived using the Hollingsworth and Lonnerberg method on o-b output from the OSTIA reanalysis v1.0. Parameters were estimated from the AATSR o-b differences for both the mesoscale and synoptic scale background error variances and background error correlation length scales, parameters estimated from the drifter o-b differences provided a valuable means of validation. The magnitude of the error variance was enhanced in regions with high SST gradients and in the marginal ice zone for both mesoscale and synoptic scale components of the background error. The observational coverage of the AATSR instrument meant that seasonal calculations of the covariance parameters could be made and seasonal variability was found in the spatial patterns of both components of the error variance.

The correlation length scales showed less seasonal variability but the length scales were found to be latitudinally variable with an increase in the length scale at the equator and at mid-latitudes in both mesoscale and synoptic scale components. Anisotropy was also found in the correlation length scales with different scales found in the East-West and the North-South directions.

The impact of the updates on the OSTIA SST analysis was tested using seasonally varying estimates of the mesoscale and synoptic scale error variances and with anisotropic latitudinally varying mesoscale and synoptic scale correlation length scales. The system was also tested with both 10 and 100 assimilation iterations. The impact of updating the error variances alone was also tested. The accuracy of the OSTIA SST analysis was validated using both assimilated drifting buoy and AATSR o-b differences globally and in ocean regions. Using the new parameters with 100 assimilation iterations resulted in a decrease in the global RMSE from 0.52 K to 0.37 K for the drifter o-b stats

and from 0.45 K to 0.37 K for the AATSR o-b stats. Using independent ARGO data to validate the analysis the global standard deviation error was decreased from 0.47 K to 0.44 K. The accuracy of the OSTIA SST analysis is normally assessed using the o-b differences to drifting buoy data; taking this value as 0.37 K, the updates to the background error covariances are within the GCOS breakthrough target for analysis accuracy of 0.4 K [RD.285]. The breakthrough target is the accuracy level, if achieved, that would result in a significant improvement for climate applications. Note that the independent ARGO comparisons are also close to the breakthrough accuracy level.

The impact of the covariance updates on the ability of the SST analysis to resolve small scale ocean features was studied using the SST gradients. The SST gradients were magnified in all the runs using the updated parameters compared to the control run. It was found that the run using the updated error variances with the old correlation length scales had slightly improved accuracy statistics both regionally and globally compared to the run with updated variances and updated correlation length scales. However investigating the feature resolution showed that the new variance-only run tended to contain noise which contaminated the SST analysis. This was not the case for the run using both updated variances and correlation length scales. It was decided to implement the updates to both covariance parameters and to increase the number of assimilation iterations from 10 to 100.

## 2.7 Future Enhancements

### 2.7.1 Enhancement 1

At present the OSTIA SST assimilation cannot read in full spatial fields of the correlation length scales. The latitudinal variability observed in section 2.3 was parameterised using a functional form. Although the functional form captured the increase of the length scales at the equator, the lengthening that was observed at mid-latitudes was not represented. In the near future the OSTIA system will transition to use the NEMOVAR [RD.283,RD.284] assimilation code in which inputting full fields of significantly smoothed correlation length scales should be feasible. We would then be able to represent the lengthening observed at mid-latitudes and could also capture the meridional variations in correlation length scales observed across ocean basins which were lost when the zonal averages presented here were calculated.

### 3. SEA ICE AND SST CONSISTENCY

#### 3.1 Introduction

As detailed in the OSTIA reanalysis technical report [RD.275] and accompanying paper [RD.239], the consistency between the OSTIA sea ice extent and the analysis freezing SST extent is at times poor. In the Southern Hemisphere, the consistency is good apart from in the summer months, where the ice extent is greater than the freezing SST extent. However, in the Northern Hemisphere, the ice extent is greater than the freezing SST extent at all times of the year. The purpose of this work is to try to reduce this discrepancy, by adjusting the current relaxation method used in OSTIA.

#### 3.2 Methods

The problem of inconsistency between the sea ice and SST datasets occurs when both datasets indicate different freezing extents. As the SST data is sparse at high latitudes and is likely to include various biases, here the ice concentration is assumed to be the most accurate. In this study, the sea ice concentration dataset (OSI-SAF ice concentration reprocessing dataset, v1.0, [RD.43]) has been used to attempt to force the analysed SSTs (re-runs of OSTIA reanalysis v1.0, [RD.239]) to match. It is possible, given the differences between the OSI-SAF dataset and other ice concentration datasets [RD.239] e.g. HadISST1 [RD.74], that there are biases in the sea ice concentration data, but in the absence of a “true” dataset, the OSI-SAF data is assumed reliable. The existing method used in OSTIA was adapted to try to force the SSTs to match the freezing extent indicated by the ice concentration information.

The OSTIA system includes a relaxation to freezing temperature (-1.8°C) under ice with a concentration of >50%. This is performed when producing the SST background at the same time as the relaxation to climatology [RD.275]. The relaxation under ice is conducted on an e-folding timescale linearly dependent on the ice concentration itself. For an ice concentration of 100% the relaxation timescale will be 5 days, and for 50% it will be 17 days. For ice concentrations of <50% the relaxation is to SST climatology rather than freezing.

For this sensitivity study the relaxation timescales and the minimum ice concentration for this relaxation were adjusted, and the impact on the ice and freezing temperature extents was investigated. The default values of the relaxation timescale and minimum ice concentration for the relaxation to freezing temperature are set to 5 days and 50%. In the sensitivity study, the timescale was varied to 1 day and 9 days, holding the minimum ice concentration at 50%, and then holding the timescale at 5 days, the ice concentration was set to 15% and 35%. A summary of these runs is given in Table 3.1.

Run Name	e-folding relaxation timescale	Minimum ice concentration for relaxation to freezing
Control (default)	5 days	50%
Run A	1 day	50%
Run B	9 days	50%
Run C	5 days	15%
Run D	5 days	35%

Table 3.1 Summary of sensitivity runs

In the Northern Hemisphere in summertime especially, freezing temperatures are spatially very variable owing to variations in salinity, mostly due to the influx of fresh water from large rivers. This affects regions such as along the Siberian coast. However, a single value for the freezing temperature is currently chosen for the method used in the OSTIA system. The mean freezing temperature for the Arctic (for >58°N) calculated from a 3-month salinity climatology (PHC 3.0, [RD.277]) gives a value of -1.65°C in summer and -1.77°C in winter. For the Antarctic (>58°S), the mean freezing temperature is -1.87°C for both summer and winter. Therefore the -1.7°C extent has been used in the comparisons made below (figure 3.1 and in subsequent figures) as the mean freezing temperature for the Northern Hemisphere. Additionally, although the SSTs are being relaxed towards -1.8°C in OSTIA, this is an asymptotic value so -1.7°C should include all the temperatures at or near freezing, hence the decision to also use this value for the Southern Hemisphere.

### 3.3 Results

#### 3.3.1 Timeseries

Figure 3.1 shows the timeseries for 2005 of the ice extent and freezing temperature extent of the various sensitivity experiments (see table 3.1).

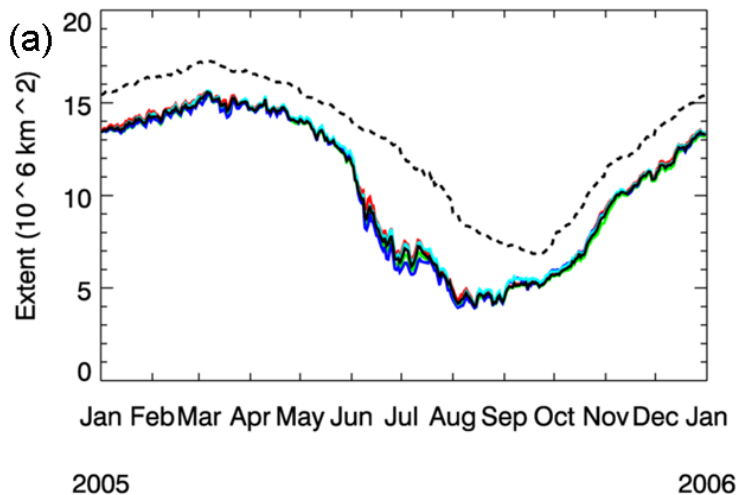


**Figure 3.1. Daily OSTIA ice and freezing SST extents (in  $10^6 \text{ km}^2$ ) for 2005, for (a) Northern Hemisphere and (b) Southern Hemisphere. Freezing SST is assumed to be  $-1.7^\circ\text{C}$  for both hemispheres.**

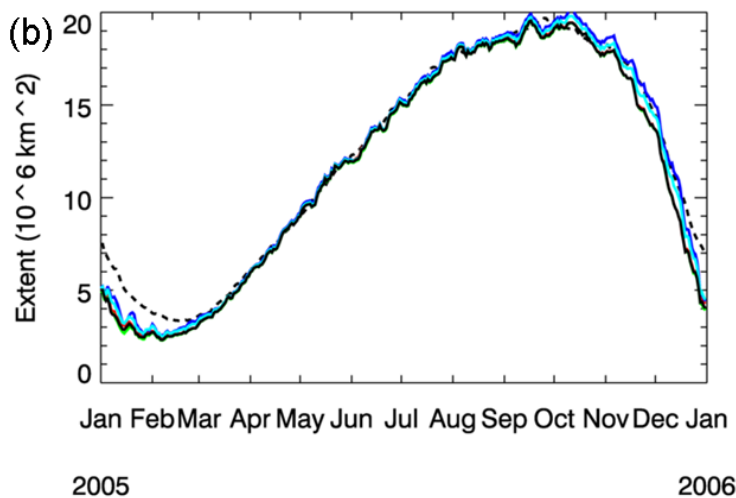


Figure Legend	
black:	Control
red:	Run A
green:	Run B
dark blue:	Run C
light blue:	Run D
dashed black:	ice extent 15%

Figure 3.1 indicates there is little effect on the magnitude of the overall SST freezing extent by altering the relaxation timescale and minimum ice concentration for relaxation to freezing. It is not possible to force the SST and sea ice to match using this method. It is also interesting to note that there are some non-linear effects taking place, for example the relaxation using 15% ice concentration in the Northern Hemisphere produces a generally smaller freezing SST extent than the default 50%, whereas using 35% produces a generally larger freezing extent. However, the differences between the runs are very small for both hemispheres. In the Southern Hemisphere, where there is already better agreement between the sea ice extent and SST freezing extent the sensitivity test fails to improve the mismatch seen in the Southern Hemisphere summer, where the freezing extent is smaller than the ice extent.

### 3.3.2 SST and Sea Ice Scatter Plots

The results from the sensitivity study runs were also plotted in the form of SST and sea ice scatter plots to investigate the relationship between the two variables. Plots were generated for 01 March 2005 and 01 September 2005 for both hemispheres. These dates correspond to months with maximum or minimum ice extents, depending on the hemisphere. Low resolution plots (1/4 degree) are shown here, as the density of points on the full resolution plots (1/20 degree) means patterns are less clear.

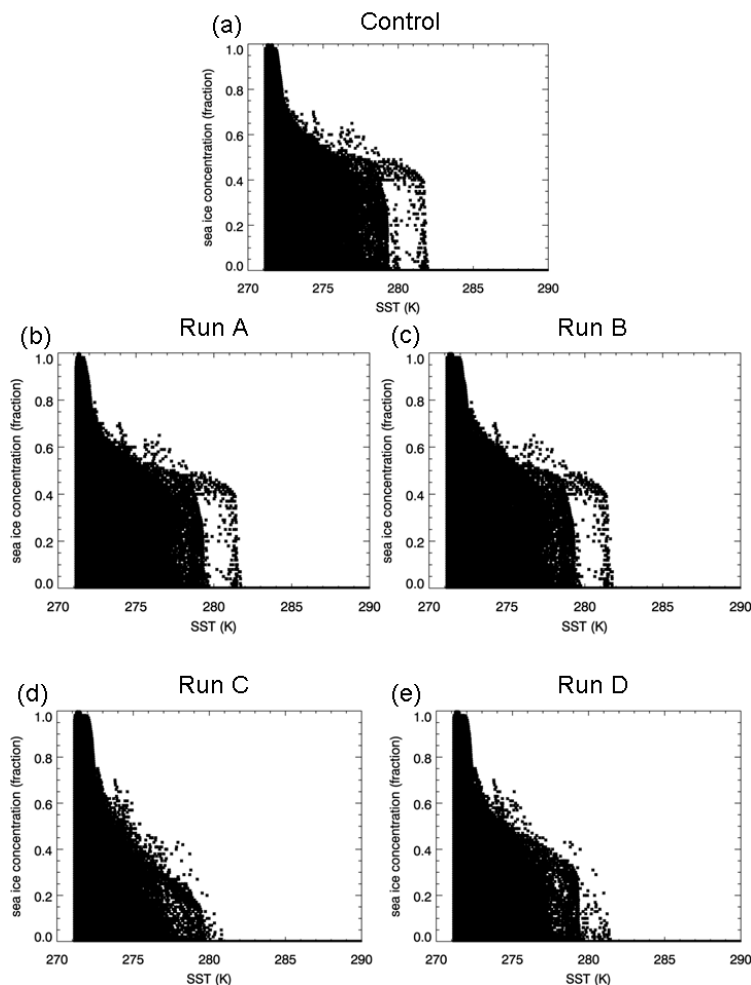


Figure 3.2 SST and sea ice concentration scatter plots for Northern Hemisphere, on 01 March 2005, where (a) Control, (b) Run A: Relaxation e-folding timescale 1 day, (c) Run B: Relaxation e-folding timescale 9 days, (d) Run C: Minimum concentration for relaxation 15%, (e) Run D: Minimum concentration for relaxation 35%.

Figure 3.2 shows that results from Run C have fewest outliers from the main band, and this run therefore produces the best results. For this run, the ice concentration above which the relaxation to freezing begins was lowered from 50% to 15%. The second best run was Run D, where the ice concentration for relaxation was lowered to 35%. Adjusting the ice concentration threshold for relaxation to freezing temperature smoothes the SST-sea ice relationship at lower concentrations, i.e. lower than 50%, as seen by comparing the distribution of points below these thresholds for figures 3.2a (50%), 3.2d (15%) and 3.2e (35%). The runs where the relaxation timescales were altered (3.2b, 3.2c) show little difference to the control, using this metric. At very high ice concentrations (~98%-100%) the minimum temperature is  $-1.8^{\circ}\text{C}$ , whereas at lower ice concentrations the minimum SST can reach  $-2.0^{\circ}\text{C}$ , the minimum set in the OSTIA reanalysis. The temperature is able to dip below  $-1.8^{\circ}\text{C}$  owing to negative increments added during the assimilation procedure. Presumably the location of the very high ice concentrations at the centre of the ice pack means negative increments do not reach these SSTs.

A similar pattern for the SST and sea ice relationships was seen for the Southern Hemisphere (figure 3.3), but with a narrower distribution compared to the Northern Hemisphere (figure 3.2). The Southern Hemisphere plots for September (not shown) look very similar to those for March (figure 3.3), but the September data for the Northern Hemisphere (not shown) show a larger variance than seen for March on figure 3.2.

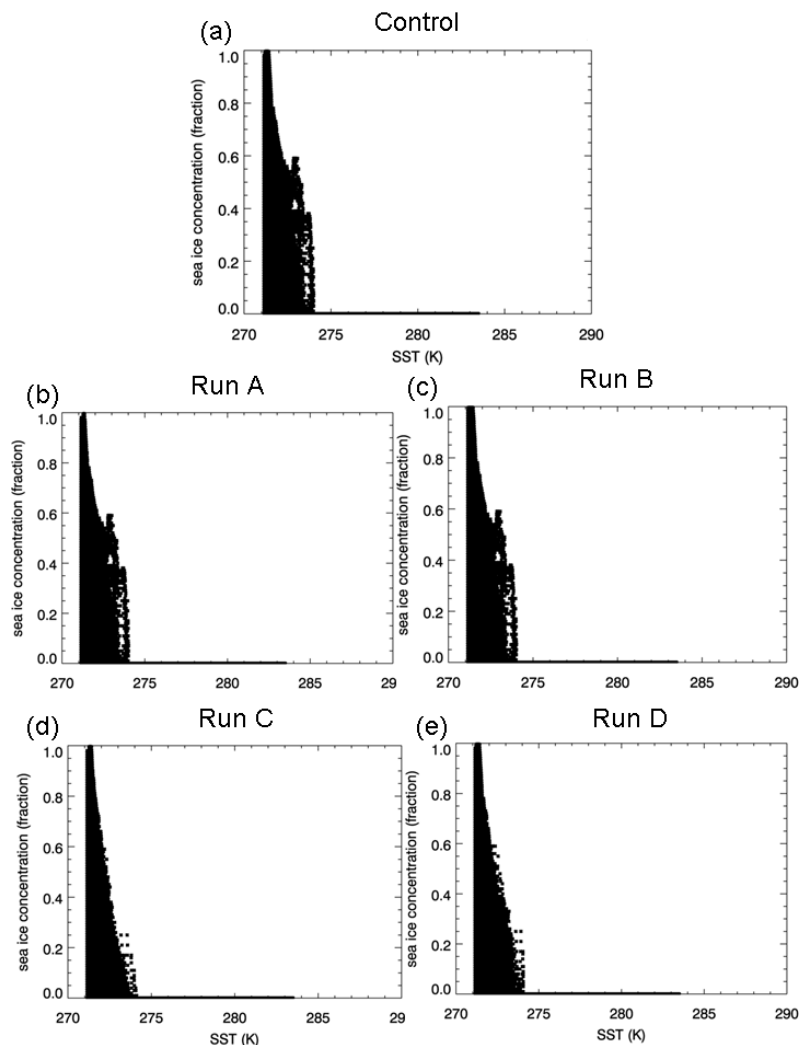
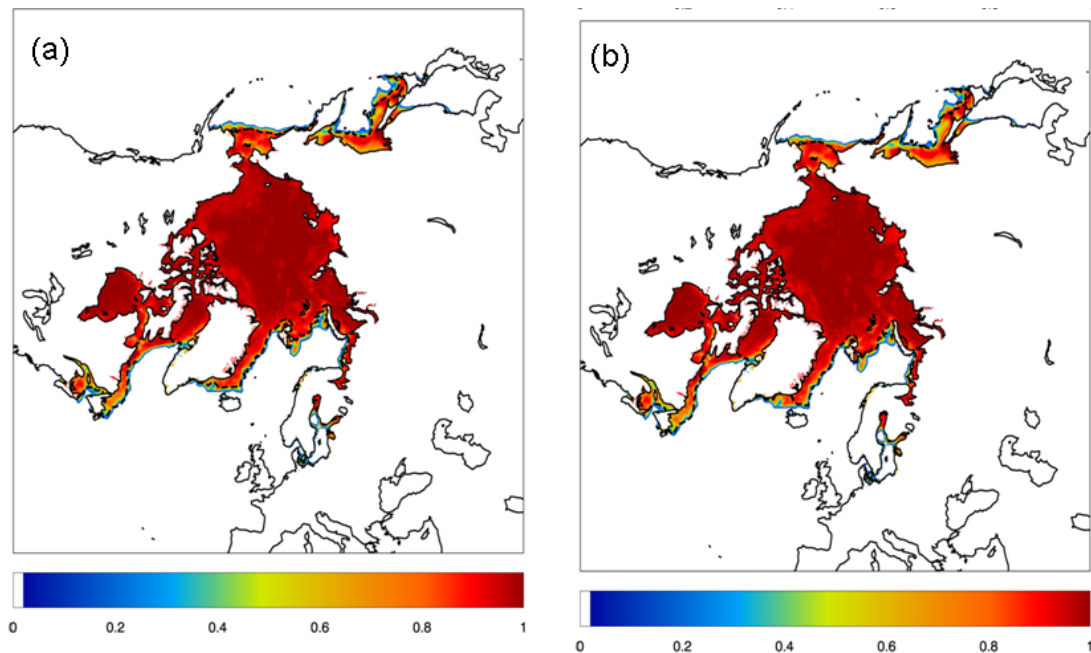


Figure 3.3 As in figure 3.2, but for Southern Hemisphere on 01 March 2005.

Although the sensitivity tests make little difference to the overall ice extent, (figure 3.1) local effects can be seen around the ice edge. This is illustrated for run C in figure 3.4 which shows the freezing extent with the ice concentration spatially for an example date in March 2005. Using the 15% concentration level for relaxation improves the match in some locations, e.g. the Sea of Okhotsk, but this alteration of the SST is actually detrimental to the matching in others. This negative effect can be seen in regions such as between Iceland and Greenland, and the ice across the Bering Strait. This is better for the run using 35% concentration for relaxation (not shown). This mismatch seen in figure 3.4(b) may potentially be caused by specifying  $-1.7^{\circ}\text{C}$  as a freezing temperature. It is possible that use of a salinity climatology to determine local freezing temperature may enable the freezing extents determined by the SST and sea ice fields to better match.



**Figure 3.4 Northern Hemisphere, 01 March 2005. Freezing SST ( $-1.7^{\circ}\text{C}$ ) (dashed line) and sea ice fraction (filled contours) for (a) control run, (b) run C where the minimum ice concentration for relaxation is 15%.**

### 3.4 Conclusions

It is not possible to force the sea ice extent and freezing SST extent to match by altering the relaxation timescales and the minimum ice fraction at which relaxation to freezing occurs. However, on local scales, the consistency between ice concentration and freezing SST can be improved by lowering the minimum ice concentration for relaxation from 50% to 15%, but this can have a detrimental effect on the match in other regions. Therefore other methods of improving this mismatch will be investigated.

### 3.5 Future Enhancements

In order to remove outliers which do not fit the SST/ice concentration relationship as shown in e.g. figure 3.2, a maximum SST for a corresponding ice concentration could be introduced. This method is similar to that used in HadISST1 [RD.74] and by [RD.281] who combined SST and sea ice data to make a boundary dataset for an atmospheric model. However, in the latter case, SST data were considered more reliable than the sea ice data, especially in the pre-satellite era. However, in this case we could retain the sea ice concentration data and make corrections to the SST data, as was performed for HadISST1 [RD.74].

An equation based on HadISST1 was developed by [RD.281] to determine the maximum suitable SST for a given ice concentration. However, the relationship between ice concentration and SST given by this equation does not match that of the OSTIA data. Additionally, any method whereby the OSTIA SSTs are artificially altered needs careful validation to ensure artificial SST gradients are not introduced near to the ice edge.

Currently, the under-ice temperature for relaxation is set to  $-1.8^{\circ}\text{C}$  in both hemispheres. However, this freezing temperature is dependent on the salinity of the water. As mentioned above, the mean freezing temperature of the Arctic is  $-1.7^{\circ}\text{C}$ . Therefore temperatures in the Arctic could be relaxed towards  $-1.7^{\circ}\text{C}$  rather than  $-1.8^{\circ}\text{C}$ . A further improvement would be the use of a spatially varying salinity climatology, which would allow the freezing temperature beneath the ice to vary regionally.

It will be interesting to see in the new CCI reanalysis how corrections to high latitude SST biases affect the consistency between the ice extent and freezing SST in OSTIA. Also, as this version of the OSTIA reanalysis will not use the ICOADS in situ dataset, this data will be available for, among other uses, the investigation of biases in high latitude SSTs.

It is likely that some of the mismatch between ice and SST freezing extents is due to the information from the SST observations being spread too far into the ice pack. This could be improved by altering the length scales used to propagate this information. The length scales would need to change according to the location of the varying edge of the sea ice which would be complicated to include. However, a simple experiment where the length scales are altered globally could be conducted, and the results in the high latitudes investigated to assess the effect these changes are likely to have. Another possible method to improve the mismatch would be to assimilate pseudo-observations of freezing temperature in regions covered by ice, which would prevent SST data from spreading underneath the ice. This would constitute a large number of data points however. Issues related to this could be avoided by subsampling the pseudo-observations or only using pseudo-observations in the marginal ice zone.

As discussed in [RD.275], it is not necessarily expected that the ice and freezing SST extents should match exactly, especially in summer. It may be useful to compare the OSTIA SST-sea ice relationship with model output, to further investigate this relationship.



## 4. PRE-PROCESSING SEA ICE DATA

### 4.1 Introduction

The OSI-SAF global sea ice concentration reprocessing dataset [RD.43] will be used for the OSTIA CCI reanalysis. However, there are a number of data gaps, ranging in length from one day to several weeks, resulting from either lack of available data, missing data within the ice field or rejection through our own quality control. For the previous version of the OSTIA reanalysis (v1.0), ice concentration from the previous available day was persisted in the event of a data gap. For gaps of 7 days or longer, the ice concentration file at the end of the data gap was copied to the centre and persisted to the end of the gap [RD.275]. The aim of this work is to improve upon this persistence method, using a simple linear interpolation method based on data assimilation theory to fill the sea ice timeseries gaps.

### 4.2 Method

For each location on the ice concentration grid, we require an ice concentration estimate for each day of the gap. This estimated ice concentration is weighted by the error estimates of the data at either end of the gap, as well as its relative temporal position in the gap. This is achieved using the following method.

A linear model is used for the interpolation of data into the time gap, of the form  $y = mt + c$ , where  $y$  are the observations of ice concentration at a particular grid point at different times  $t$ , in days. The linear model for the interpolation ( $y = mt + c$ ) is put into matrices to give the model value at observation times.

Using data assimilation theory, e.g. [RD.276], a cost function  $J$  can be derived:

$$J = (y - Hx)^T R^{-1} (y - Hx) \quad (4.1)$$

Minimising equation (4.1) with respect to  $x$ , and rearranging for  $x$  gives

$$x = (H^T R^{-1} H)^{-1} H^T R^{-1} y \quad (4.2)$$

where

$$H = \begin{bmatrix} t_1 & 1 \\ t_n & 1 \end{bmatrix}, \quad x = \begin{bmatrix} m \\ c \end{bmatrix}, \quad y = \begin{bmatrix} y(t_1) \\ y(t_n) \end{bmatrix}, \quad R = \begin{bmatrix} V_1 & 0 \\ 0 & V_n \end{bmatrix}$$

$t_1$  is day 1, the day available at the start of the gap, and  $t_n$  is the day at the end of the gap of length  $n$  days.  $x$  are the parameters in the linear model which determine the best estimate of ice concentration.  $R$  is the observation error, where  $V_{1,n}$  is the variance of the observation errors at  $t_{1,n}$  (provided with the data).

Then we can use  $x(0) = m$  and  $x(1) = c$  in the model equation for any  $t_n$  in the gap, to find the ice concentration ( $y$ ) at this point. It is assumed errors at the start and end of the period are uncorrelated.

### 4.3 Results

Tests were run using OSI-SAF sea ice reprocessing data [RD.43] between 26 May 2002 and 31 May 2002, for both the Northern and Southern Hemispheres. These dates were chosen at random. The method described above was used to generate ice concentration fields for four days where complete fields were already available, for comparison.

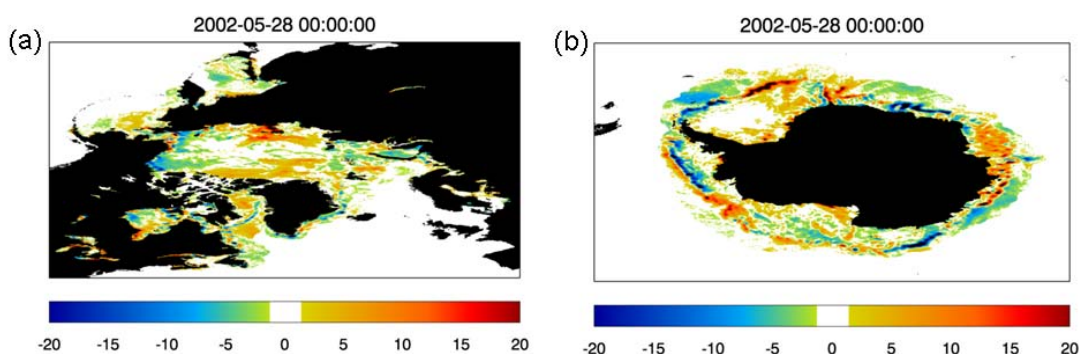


Figure 4.1. Interpolated minus real ice concentration field (%) on 28 May 2002, for (a) Northern Hemisphere and (b) Southern Hemisphere.

Date	Northern Hemisphere RMSE (mean error) of absolute concentration differences, %		Southern Hemisphere RMSE (mean error) of absolute concentration differences, %	
	Interp – real	Persist – real	Interp – real	Persist – real
20020527	3.81 (2.22)	4.16 (2.39)	3.97 (2.50)	4.65 (2.80)
20020528	4.53 (2.76)	5.58 (3.32)	5.61 (3.46)	7.55 (4.34)
20020529	4.52 (2.71)	6.44 (3.83)	5.21 (3.27)	9.07 (5.11)
20020530	4.03 (2.20)	7.37 (4.37)	3.44 (2.20)	10.08 (5.48)

Table 4.1 : Ice concentration difference statistics (absolute differences). Persistence method uses file from 20020526. Statistics calculated using gridpoints where ice is present in either file.

Figure 4.1 shows the difference between a sample interpolated field and the actual field for both hemispheres. The low ice concentration data outside of the ice edge seen on figure 4.1 are erroneous and are filtered out in the OSTIA reanalysis according to guidance in the OSI-SAF user manual [RD.43]. The differences between the real and interpolated fields are largest around the ice edge (figure 4.1), which is the region where the largest day-to-day (and potentially non-linear) changes would be expected, and is hence the most difficult to capture using a linear interpolation method. Figure 4.1 illustrates that the differences are spatially variable, but the overall mean differences are small, as shown in table 4.1. This table gives the differences between both the interpolation and persistence methods and the observed (real) ice concentration. We would expect to see some differences between the real and interpolated fields since in reality the ice concentration does not change according to the linear model used and the rate of change is probably dependent on the time of year. However, these differences are smaller than were found for the persistence method (table 4.1), demonstrating that even using a changing ice concentration field based on a linear approximation is an improvement over persisting the ice concentration field from the start of the data gap. Note that the errors of the persisted compared to the real ice concentration field continue to grow with time, whereas the magnitude of the errors remains steady for the interpolation method (table 4.1).

Overall, the differences between the real and interpolated fields are small, and as they are of a similar magnitude to the day-to-day variation of the real ice concentration fields for this time period (not shown) the results show the test is successful.

## 4.4 Conclusions

The method works well and produces good results. It has been used to produce interpolated data for the gaps in the OSI-SAF ice concentration timeseries between 1991 and 2007, which will be used in the CCI reanalysis Level 4 product.

## 4.5 Assumptions and Limitations

Error information in the sea ice files is passed through to the final OSTIA output files (see section 5.1). However, when the field is interpolated, the error information is set to missing data as no information is available. Status flags are assigned as a separate field to the error information and have been set as 100 for land, 12 for sea and 13 for interpolated ice concentration data, following the OSI-SAF convention for this dataset. For all the interpolated data within a gap, the overall ice extent (where there is any ice above 0%) does not change. This is because there is always ice above 0% where there is ice in either the start or end files. If the minimum is set to 15% for flagging as interpolated ice concentration data, the ice area does change in the files, but it has been set to 0% to keep the OSI-SAF convention.

This method works best for shorter gaps. The greater the difference between the ice fields at the start and end of the gap, the poorer the results.

## 4.6 Future Enhancements

A few incomplete fields are available which were removed as part of the quality control. These could be used to add a spatial interpolation component to the method.

## 5. USE OF SEA ICE DATA AUXILIARY INFORMATION

### 5.1 Error Estimates

#### 5.1.1 Background

Version 1.1 of the OSI-SAF ice concentration reprocessing dataset [RD.43], to be used in the OSTIA CCI reanalysis, includes error estimates for each point on the 10 km polar-stereographic OSI-SAF grid. It is useful to be able to include this error information along with the OSTIA ice concentration data in the final Level 4 product files. An SST error estimate is already included in the OSTIA files.

The total error estimate provided in the OSI-SAF reprocessing dataset is made up of an algorithm error and a representivity (or “smearing”) error. The algorithm error can be easily interpolated onto the OSTIA grid, but the representivity error is dependent on the size of the grid, as it is related to the spreading of information from the satellite footprint to the grid. It is not trivial to calculate a representivity error for the OSTIA grid - the method used by the OSI-SAF involves using MODIS images for comparison. It is not practical to use a similar method to recalculate the OSTIA error, so the decision was taken to simply interpolate the total error estimates onto the OSTIA grid. This will introduce an uncertainty in the representivity error component, the magnitude of which is unknown (R. Tonboe, 2012, pers. comm.). However, as we are moving from a larger grid (OSI-SAF 10 km) to a smaller grid (OSTIA ~6 km) it is possible that the magnitude of the representivity error will decrease. Therefore it can be inferred that this uncertainty should not increase the total error estimate provided.

#### 5.1.2 Method

The total error estimate given in the OSI-SAF files is read in to OSTIA alongside the ice concentration information itself, regridded on to the OSTIA grid and written with the OSTIA SST and ice concentration data to the Level 4 product file.

The total error is simply a sum of the representivity error and the algorithm error components which are provided separately in the OSI-SAF files, along with the total error variable. For both of these separate error types, data outside of the ice region is set to missing data. For the total error data, this error over the ocean is set to 7% in the OSI-SAF files, a figure derived from the literature (R. Tonboe, 2012, pers. comm.). Error information for the open ocean is useful for capturing uncertainties in the ice edge, especially for applications such as data assimilation. However, the OSTIA ice concentration field is a global field, and to have an ice uncertainty of greater than zero in permanently ice-free latitudes is not suitable.

A method to check the distance from the ice edge for each point and to decrease the ice error according to a formula could be computationally expensive, and the time to develop such a method is disproportional to the minor benefits to be gained. Therefore, open water data within the OSI-SAF grid is assigned an error of 7%, as in the OSI-SAF files, and all ocean outside this region is assigned an ice error of 0%. It was agreed by the OSI-SAF that setting the open ocean uncertainty to 0% outside of the OSI-SAF grid and 7% inside is a sensible procedure (R. Tonboe, 2012, pers. comm.).

#### 5.1.3 Assumptions and Limitations

Ice concentration fields for gaps in the timeseries filled in by a data assimilation interpolation method (section 4) have no error information. During the OSTIA processing, the interpolated field is therefore assigned the maximum error estimate, taken from the OSI-SAF files. However, this maximum error differs between the Northern and Southern

Hemispheres, at 13% and 18% respectively. The same algorithm is used in both hemispheres, so this difference must result from differing tie-point errors used in each hemisphere (R. Tonboe, 2012, pers. comm.). For the global OSTIA ice concentration error field, the error for interpolated data should not differ between the Northern and Southern Hemispheres. Therefore the maximum error was chosen, 18%, for both hemispheres. This value will also appear in the OSTIA ice error information for the OSI-SAF fields occasionally in the field itself, but also where there has been interpolation conducted by OSI-SAF around the pole region or coasts, or because of missing data within the ice pack, where no other error estimates are supplied.

The difference in resolution between the OSTIA and OSI-SAF grids means filling around the coastlines is required. This is performed in addition to the OSI-SAF interpolation around the coasts already conducted. Hence the error is set to 18% around coasts, as for other interpolated data. However, coasts in regions of open water which are still on the OSI-SAF grid, such as around the UK, will also be assigned errors of 18%. Clearly sea ice is not expected to form in this region so it should be noted errors in these regions are too high.

#### 5.1.4 Conclusions

A new field called `sea_ice_fraction_error` will be included in the new OSTIA files for the CCI reanalysis. This is a regridding of the OSI-SAF ice error information. Interpolation alters the uncertainty information but effects on the error estimates themselves are estimated to be small.

## 5.2 Status Flags

### 5.2.1 Background

The status flags provided with the OSI-SAF sea ice concentration reprocessing dataset [RD.43] may indicate the data has been corrected, while others indicate potentially suspect data. A list of the status flag descriptions taken directly from the NetCDF header information in the sea ice files is given below:

- 0 - nominal value from algorithm used
- 1 - t2m check indicates possibly false ice
- 2 - over lake caused possibly less accurate
- 10 - value changed by coast correction method
- 11 - value changed by applying maximum climatology
- 12 - missing value set by applying maximum climatology
- 13 - value set by applying interpolation
- 100 - missing value due to over land
- 101 - missing value due to missing data

For the OSTIA reanalysis it is useful to use the corrected data, for example, interpolation over areas of missing data such as the pole hole is performed by the OSI-SAF using spatial and temporal interpolation weighted according to the error in the data [RD.43]. This is an improvement over the simple bilinear spatial interpolation used for gaps in sea

ice information in the operational OSTIA system. Similarly, other changes to the ice concentration based on e.g. maximum climatological ice extent are useful.

Ice concentration data failing the 2m air temperature check is not automatically removed from the OSI-SAF dataset. The effect of removing this data on the ice extent is investigated in the following section. In addition, a check on the coastal correction method has been performed and the suitability of retaining the lake ice information has been assessed.

### 5.2.2 2m air temperature flag

Sea ice flagged as questionable in the OSI-SAF dataset owing to failing the 2m air temperature check (where air temperature  $> +10^{\circ}\text{C}$ ) was removed. This is not carried out automatically by OSI-SAF, unlike for the other checks. One year (2005) of the OSTIA reanalysis v1.0 [RD.239] was re-run to assess the difference the use of this status flag makes to the total ice extent. The use of the 2m air temperature flag removes spurious ice observations around the coast in the Northern Hemisphere summer, see for example figure 5.1(a). The removal of this spurious ice is large enough to make a difference to the overall summertime Arctic ice extent (figure 5.1(b)).

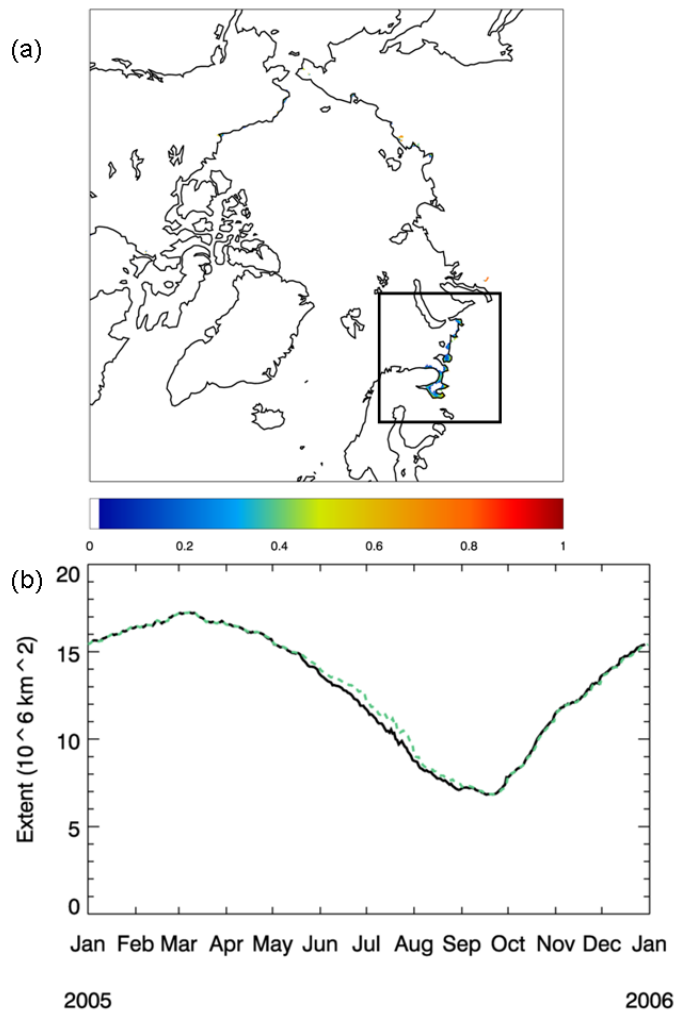


Figure 5.1. (a) OSTIA ice concentration field for 15 August 2005. Data without 2m air temperature ice concentration check minus data with all points failing this check set to 0% ice concentration. Box shows main area affected. (b) 2005 daily ice extent for Northern Hemisphere with (black) and without (dashed green) 2m air temperature check.

### 5.2.3 Coastal correction method

For the OSI-SAF ice concentration reprocessing data, correction of data in the coastal zone has been undertaken by the OSI-SAF [RD.43]. In the operational OSTIA system it is necessary to perform filling of missing data at the coast using a simple two-dimensional linear interpolation method. There are some very small differences between the results using the two methods, and as the OSI-SAF procedure is likely to be more accurate than the simple filling performed by the OSTIA system, sea ice data with a flag of 10 will be included in the OSTIA reanalysis.

Although the coastal filling using the OSI-SAF method will be included, some spatial filling around coastlines is still required to ensure there are no regions of missing data where there is a mismatch of coastlines between the high resolution OSTIA and lower resolution OSI-SAF dataset.

### 5.2.4 Lake ice flag

The OSI-SAF ice concentration dataset also includes a lake ice product. However, there are a number of days in the summer months where this dataset indicates spurious ice cover over the lakes, see for example figure 5.2. Note particularly the North American Great Lakes which should be ice-free at this time of year. This issue is potentially caused by cloud contamination. As the status flags are not cumulative this lakes data will not be flagged as also having failed the 2m air temperature check. The decision has been taken to include lake surface temperatures in the OSTIA CCI reanalysis, but to not use the OSI-SAF lake ice product. Therefore data with a flag of 2 will be removed. There is no ice information over the Caspian Sea or the Black Sea as they are outside of the OSI-SAF polar-stereographic grid.

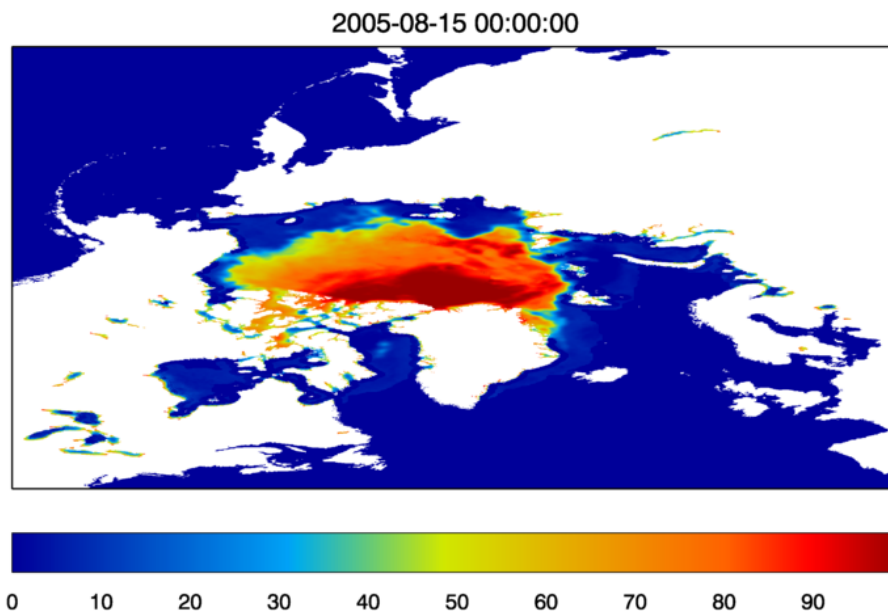


Figure 5.2. OSI-SAF Northern Hemisphere ice concentration, 15 August 2005

### 5.2.5 Conclusions

Sea ice concentration flagged as failing the 2m air temperature check will be removed (set to 0% ice concentration) and not used in the CCI reanalysis. Ice concentration flagged as over lakes will also be removed. The other OSI-SAF status flags will not be used to alter the default data.

## 6. SUMMARY

The OSTIA reanalysis system has been improved in preparation for producing the CCI SST Level 4 product. New background error covariances have been calculated using (A)ATSR observations to enhance the SST analysis. The background error covariances are now based on observations and attempt to capture both seasonality in the variances, and the anisotropy and latitude dependency of the correlation length scales. This is a major improvement on the old system which used values based on model output, and two single values for correlation length scales. The analysis has been further developed by increasing the number of analysis iterations which improves the resolution of small scale features. Sensitivity experiments have shown that the new background errors and increased number of iterations improve the accuracy of the OSTIA system. The drifting buoy o-b RMSE is reduced from 0.52 K to 0.37 K in the improved system, below the GCOS breakthrough target for analysis accuracy of 0.4 K, even though the improvements to the input SST data expected from the other CCI SST work have not yet been included. When compared to the independent ARGO data, the standard deviation error reduces by a smaller amount from 0.47 K to 0.44 K. Experiments using the old correlation length scales show even further improvements in accuracy, however, inspection of SST gradient plots revealed that temporal observational noise was present in the results. Therefore, the new correlation length scales, together with the new variances and increased number of iterations will be used in the new OSTIA reanalysis system. These changes will also be carried through to the NRT OSTIA system.

Work has also been carried out to improve the use of the sea ice data in OSTIA. The sensitivity of the SST analysis to the relaxation parameters used under ice was investigated to try to improve the consistency between the sea ice data and SST analysis; however, it was found that the sea ice and SST fields could not be made more consistent by changing the parameters. Future work has been suggested to improve the consistency, which includes using a spatially varying freezing temperature field in OSTIA and also changing the length scales used in the analysis around the ice edge to stop SST observations spreading too far under the ice pack. A method based on assimilating pseudo-observations of freezing temperature underneath the ice has also been suggested. It will be interesting to note whether improvements in the input data sources for the CCI project reduce the discrepancy between the SST analysis and ice concentration data for this new version of the OSTIA reanalysis.

A method to fill a number of data gaps in the sea ice dataset used in the OSTIA reanalysis has been developed and shown to successfully complete the sea ice record. This will be implemented in the OSTIA reanalysis system. This method cannot be directly used in the NRT system as it requires knowledge of the sea ice in the future, but a similar method is planned for the operational system.

Finally, work has been carried out to make greater use of the auxiliary information supplied with the sea ice concentration data. Error estimates for the concentration data supplied with the sea ice dataset will now feature in the final OSTIA Level 4 files, when the OSI-SAF ice concentration reprocessing sea ice dataset [RD.43] is used. (The error estimates are not available in the corresponding OSI-SAF operational product.) Additionally, the quality control process in the OSTIA system will use additional status flags in the sea ice data set to reject poor data.

In summary, the OSTIA reanalysis system has been improved in preparation for producing the CCI SST Level 4 product. The developments have led to an increased accuracy of the SST analysis and greater use of the sea ice data.